THE ASTROPHYSICAL JOURNAL, 415:589–615, 1993 October 1

SN 1992A: ULTRAVIOLET AND OPTICAL STUDIES BASED ON *HST*, *IUE*, AND CTIO OBSERVATIONS[1]

ROBERT P. KIRSHNER,[2] DAVID J. JEFFERY,[2] BRUNO LEIBUNDGUT,[2,3] PETER M. CHALLIS,[2] GEORGE SONNEBORN,[4] M. M. PHILLIPS,[5] N. B. SUNTZEFF,[5] R. CHRIS SMITH,[5] P. FRANK WINKLER,[6,7] CLÁUDIA WINGE,[7,8] MARIO HAMUY,[5] DEIDRE A. HUNTER,[7,9] KATHERINE C. ROTH,[7,10] J. C. BLADES,[11] DAVID BRANCH,[12] ROGER A. CHEVALIER,[13] CLAES FRANSSON,[14] NINO PANAGIA,[11] ROBERT V. WAGONER,[15] J. CRAIG WHEELER,[16] AND ROBERT P. HARKNESS[16]

Received 1993 January 27; accepted 1993 March 31

ABSTRACT

The Type Ia supernova SN 1992A in the S0 galaxy NGC 1380 was observed as a target of opportunity by the *International Ultraviolet Explorer* (*IUE*) and with great alacrity by the *Hubble Space Telescope* (*HST*). Here we present the *HST* and *IUE* spectra and photometry that we obtained, as well as optical spectra obtained at the Cerro Tololo Inter-American Observatory (CTIO). The *HST* Faint Object Spectrograph (FOS) spectra, from 5 and 45 days past maximum light, are the best UV spectra of a Type Ia supernova and reveal for the first time with good signal-to-noise ratio the Type Ia spectral region blueward of ~2650 Å. The UV photometry taken in the F175W, F275W, and F342W bands defined by the *HST* filters shows light curves that resemble the Type Ia template *U* light curve. Using data from SN 1992A and SN 1990N, we have constructed a Type Ia template light curve for the flux region near 2750 Å that is quite detailed from 14 days before maximum light to 22 days after maximum light and that extends to 77 days after maximum light. This light curve also resembles the template *U* light curve. A high-resolution *HST* Goddard High Resolution Spectrograph (GHRS) spectrum of SN 1992A shows no evidence for any interstellar lines attributable to NGC 1380 or to Galactic high-velocity clouds; low-velocity Galactic gas gives rise to relatively weak Mg II UV resonance absorption lines. These results are consistent with low extinction along the line of sight to SN 1992A.

We have done a parameterized LTE analysis of the SN 1992A spectra using a slightly modified version of Woosley's delayed-detonation model DD4. We find that the features in the region blueward of ~2650 Å in the *HST* spectra are P Cygni absorptions due to blends of iron peak element multiplets and the Mg II resonance multiplet. Newly synthesized magnesium, sulfur, and silicon probably extend to velocities at least as high as ~19,000 km s^{-1}. Newly synthesized Ni-Co may dominate the iron peak element abundances out to ~13,000 km s^{-1} in the ejecta of SN 1992A as in model DD4. However, further investigation of the extent of Ni-Co material in SN 1992A and other Type Ia supernovae is needed; this investigation could greatly help constrain Type Ia models.

An analysis of the O I λ7773 line in SN 1992A and other Type Ia supernovae implies that the oxygen-rich layer in typical Type Ia's extends over a velocity range of at least ~11,000–19,000 km s^{-1}. None of the explosion models we considered, including model DD4, has an oxygen-rich layer that completely extends over this range. Model DD4, however, is promising, and further investigation of delayed-detonation models of its kind is merited.

Spectropolarimetric observations taken by Spyromilio & Bailey of SN 1992A are consistent with the SN 1992A being spherically symmetric. We discuss these observations and the importance of taking spectropolarimetry of other Type Ia supernovae.

Subject headings: galaxies: individual (NGC 1380) — supernovae: individual (SN 1992A) — ultraviolet: stars

[1] Partially based on observations with the NASA/ESA *Hubble Space Telescope*, obtained at the Space Telescope Science Institute, which is operated by AURA, Inc., under NASA contract NAS 5-26555.

[2] Harvard-Smithsonian Center for Astrophysics, MS-19, 60 Garden Street, Cambridge MA 02138.
[3] Present address: Department of Astronomy, 601 Campbell Hall, University of California, Berkeley, CA 94720.
[4] Laboratory for Astronomy and Solar Physics, NASA/Goddard Space Flight Center, Code 681, Greenbelt, MD 20771.
[5] Cerro Tololo Inter-American Observatory, National Optical Astronomy Observatories, Casilla 603, La Serena, Chile (Operated by the Association of Universities for Research in Astronomy, Inc. [AURA], under cooperative agreement with the National Science Foundation).
[6] Department of Physics, Middlebury College, Middlebury, VT 05753.
[7] Visiting Astronomer, Cerro Tololo Inter-American Observatory, National Optical Astronomy Observatories.
[8] Departamento de Astronomia, Universidade Federal do Rio Grande do Sul, Avenida Bento Gonçalves, 9500, CP15051, CEP 91501-970, Porto Alegre, RS, Brazil.
[9] Lowell Observatory, 1400 West Mars Hill Road, Flagstaff, AZ 86001.
[10] Department of Physics and Astronomy, Northwestern University 2145 Sheridan Road, Evanston, IL 60208.
[11] Space Telescope Science Institute, 3700 San Martin Drive, Baltimore, MD 21218.
[12] Department of Physics and Astronomy, University of Oklahoma, Norman, OK 73019.
[13] Department of Astronomy, University of Virginia, P.O. Box 3818, Charlottesville, VA 22903.
[14] Stockholm Observatory, S-133 36 Saltsjöbaden, Sweden.
[15] Department of Physics and Center for Space Science and Astrophysics, Stanford University, Stanford, CA 94305-4060.
[16] Department of Astronomy, University of Texas at Austin, Austin, TX 78712.

1. INTRODUCTION

Liller (1992) discovered SN 1992A in NGC 1380, an S0 galaxy in the Fornax Cluster, on 1992 January 11.16 UT. Shortly thereafter Spyromilio et al. (1992b) classified SN 1992A as a Type Ia supernova in the photospheric epoch. Photometric and spectroscopic evidence from a CTIO program of observation started on January 12 (Suntzeff & Roth 1992; Suntzeff et al. 1992, 1993) shows that SN 1992A was a typical Type Ia. The early SN 1992A *B* and *V* light curves follow the Type Ia template light curves of Leibundgut (1988, 1993) with a typical discrepancy of $\lesssim 0.2$ mag. The *B* and *V* maxima were 12.6 ± 0.2 mag and 12.61 ± 0.05 mag, and occurred on January 19.2 ± 1.0 UT and January 20.9 ± 0.5 UT. We take the epoch of *B* maximum as the maximum light of the supernova. The SN 1992A *B* and *V* maxima agree to within 0.15 and 0.25 mag, respectively, with the *B* and *V* maxima of the other Fornax Cluster Type Ia supernovae, SN 1980N and SN 1981D (Hamuy et al. 1991). A program of *IUE* spectroscopy initiated 3 days after discovery (Sonneborn & Kirshner 1992) obtained spectra in the 2650–3300 Å range that are similar to those obtained from most other Type Ia's (Benvenuti et al. 1982; Panagia & Gilmozzi 1991, Fig. 1).

Because SN 1992A was a bright Type Ia supernova with comprehensive observations beginning well before maximum light, we chose it to be the first supernova outburst to be observed with the *Hubble Space Telescope* (*HST*) under the *HST* Supernova Intensive Study (SINS) General Observer (GO) program. Astrometric measurements made on a CCD frame transferred over Internet from CTIO provided an accurate position in the Guide Star Selection System reference frame. The early *IUE* observations showed that UV observations would not be compromised by absorption in the Galaxy or in NGC 1380. With these requirements fulfilled, the *HST* observations could be executed with confidence that the target would be acquired and that good UV data would be obtained. Outstanding work at the Space Telescope Science Institute (STScI) led to prompt revisions in the *HST* schedule and observations on 1992 January 24, March 4, and April 5. On the first date, low-resolution spectroscopic observations were carried out with the Faint Object Spectrograph (FOS), a single high-resolution spectrum (useful for studying interstellar lines both in the Galaxy and in NGC 1380) was obtained using the Goddard High Resolution Spectrograph (GHRS), and Faint Object Camera (FOC) observations were done to obtain UV photometry. On March 4 only FOS observations were done, and on April 5 only FOC observations. Late-time *HST* FOC and FOS observations taken on 1992 November 5 will be reported in a forthcoming paper. A complete log of our *HST* observations of SN 1992A is given in Table 1. Table 2 gives a log of the *HST*, *IUE*, and CTIO spectroscopic observations of SN 1992A that we report on in this paper. In both tables the epoch of SN 1992A is specified relative to maximum light: e.g., day +5 means 5 ± 0.5 days after maximum light. Both for SN

TABLE 1

HST OBSERVATION LOG FOR SN 1992A THROUGH 1992 NOVEMBER 5

Date (UT)	Epoch Relative to Maximum Light (days)	Instrument	Observation Mode	Grating	Exposure Time (s)	Data Set Name
1992 Jan 24	+5	FOC (F/96)	IMAGE	F342	995.750	X0VQ0301T
1992 Jan 24	+5	FOC (F/96)	IMAGE	F275W	995.750	X0VQ0302T
1992 Jan 24	+5	FOC (F/96)	IMAGE	F175W	1806.125	X0VQ0303T
1992 Jan 24	+5	FOS/RD	ACCUM	G160L	1499.985	Y0VQ0103T
1992 Jan 24	+5	FOS/RD	ACCUM	G270H	1499.985	Y0VQ0104T
1992 Jan 24	+5	FOS/RD	ACCUM	G400H	999.990	Y0VQ0105T
1992 Jan 24	+5	GHRS	ACCUM	G270M	3916.800	Z0VQ0508T
1992 Mar 4.....	+45	FOS/RD	ACCUM	G160L	1349.989	Y0WA0202T
1992 Mar 4.....	+45	FOS/RD	ACCUM	G160L	1349.989	Y0WA0203T
1992 Mar 4.....	+45	FOS/RD	ACCUM	G270H	1349.989	Y0WA0204T
1992 Mar 4.....	+45	FOS/RD	ACCUM	G270H	1349.989	Y0WA0205T
1992 Mar 4.....	+45	FOS/RD	ACCUM	G400H	1800.000	Y0WA0206T
1992 Apr 5	+77	FOC (F/96)	IMAGE	F342W	495.750	X0WA0401T
1992 Apr 5	+77	FOC (F/96)	IMAGE	F275W	495.750	X0WA0402T
1992 Apr 5	+77	FOC (F/96)	IMAGE	F175W	995.750	X0WA0403T
1992 Nov 5.....	+291	FOC (F/96)	IMAGE	F342W	996.875	X1670201T
1992 Nov 5.....	+291	FOC (F/96)	IMAGE	F275W	996.875	X1670202T
1992 Nov 5.....	+291	FOC (F/96)	IMAGE	F175W	1996.875	X1670203T
1992 Nov 5.....	+291	FOS/RD	ACCUM	G160L	1999.980	Y1670102T
1992 Nov 5.....	+291	FOS/RD	ACCUM	G160L	1999.980	Y1670103T
1992 Nov 5.....	+291	FOS/RD	ACCUM	G160L	1999.980	Y1670104T
1992 Nov 5.....	+291	FOS/RD	ACCUM	G270H	1999.980	Y1670105T
1992 Nov 5.....	+291	FOS/RD	ACCUM	G270H	1999.980	Y1670106T
1992 Nov 5.....	+291	FOS/RD	ACCUM	G270H	1999.980	Y1670107T
1992 Nov 5.....	+291	FOS/RD	ACCUM	G400H	1999.980	Y1670108T
1992 Nov 5.....	+291	FOS/RD	ACCUM	G400H	1999.980	Y1670109T

NOTE.—The *Hubble Space Telescope* (*HST*) observations of SN 1992A were carried out under the Supernova Intensive Study (SINS) program of Kirshner et al. 1988. FOS/RD means Faint Object Spectrograph red side, FOC (F/96) means Faint Object Camera operated with focal ratio F/96, and GHRS is the Goddard High Resolution Spectrograph. Information on the *HST* instruments and observation modes can be found in the STScI instrument handbooks. For consistency the date of the observation is taken to be the date at the beginning of the observation run. The 1992 November 5 observations will be presented in a forthcoming paper.

TABLE 2

THE SPECTRA OF SN 1992A

Date (UT)	Spectral Range (Å)	Epoch Relative to Maximum Light (days)	Epoch Relative to Explosion (days)	Observatory	Observer
1992 Jan 12.058	4750–6550	−7.1	12.9	CTIO	[a]
1992 Jan 12.217	6600–8350	−7.0	13.0	CTIO	[a]
1992 Jan 13.08	3300–7600	−6.1	13.9	CTIO	[b]
1992 Jan 14.09	2000–3400	−5.1	14.9	*IUE*	[c]
1992 Jan 14.11	3550–7050	−5.1	14.9	CTIO	[d]
1992 Jan 16.18	2000–3400	−3.0	17.0	*IUE*	[c]
1992 Jan 16.25	2000–3400	−3.0	17.0	*IUE*	[c]
1992 Jan 18.91	2000–3400	−0.3	19.7	*IUE*	[c]
1992 Jan 18.97	2000–3400	−0.2	19.8	*IUE*	[c]
1992 Jan 21.58	2000–3400	+2.4	22.4	*IUE*	[c]
1992 Jan 24.141	1650–4800	+4.9	25.0	*HST*	[e]
1992 Jan 25.04	3400–8100	+5.8	25.8	CTIO	[f]
1992 Jan 27.67	2000–3400	+8.5	28.5	*IUE*	[c]
1992 Jan 28.04	3150–9900	+8.8	28.8	CTIO	[g]
1992 Jan 30.91	2000–3400	+11.7	31.7	*IUE*	[c]
1992 Feb 4.67	2000–3400	+16.5	36.5	*IUE*	[c]
1992 Feb 10.66	2000–3400	+22.5	42.5	*IUE*	[c]
1992 Mar 4.108	1800–4800	+44.9	65.1	*HST*	[e]
1992 Mar 6.03	3000–7700	+46.8	66.8	CTIO	[h]

NOTE.—For consistency the date of the observation is taken to be the date at the beginning of the exposure. In assigning the epoch relative to explosion, it has been assumed, as by Jeffery et al. 1992, that a Type Ia explosion occurs 20 days before maximum light; the maximum light of SN 1992A was 1992 January 19.2 ± 1 UT. In displayed spectra we have eliminated spectral regions with very low signal-to-noise ratio. Displayed combined spectra have been created either by addition of spectra or by joining spectra. If there was an overlap in the case of the joined spectra, we eliminated one of the two overlapping spectral regions. Only a representative selection of the *IUE* spectra are displayed (see Fig. 5 in § 6).

[a] K. C. Roth.
[b] D. A. Hunter.
[c] G. Sonneborn and R. P. Kirshner.
[d] C. Winge.
[e] R. P. Kirshner.
[f] R. C. Smith and P. F. Winkler.
[g] M. Hamuy.
[h] M. M. Phillips.

1992A and for other supernovae, we will often use this way of specifying their epochs.

The rationale of the SINS program is that intensive study of bright supernovae leads to the greatest advances in understanding supernovae. The *HST*'s unique contribution to the intensive study of supernovae caught at early epochs, such as SN 1992A, is to provide UV spectra with much better wavelength coverage, signal-to-noise ratio, and resolution than the *IUE*, and to provide UV photometry to flux limits far beyond any other instrument. *HST* observations can be carried out successfully well after maximum light, as we demonstrated by the November 5 observations.

UV spectra are important for the study of Type Ia supernovae because these spectra are formed mainly by a blanketing of iron peak element lines. In the standard exploded white dwarf picture of Type Ia's (which we adopt here; see §§ 4 and 5), the explosion ejecta below some depth has its iron peak element abundance dominated by newly synthesized iron peak elements and at a lower depth has newly synthesized iron peak elements dominating the entire composition. Most of the newly synthesized iron peak element matter is radioactive ^{56}Ni which decays according to the decay chain $^{56}\mathrm{Ni} \rightarrow {}^{56}\mathrm{Co} \rightarrow {}^{56}\mathrm{Fe}$ with half-lives of 6.10 and 77.12 days for the first and second decays, respectively (Huo et al. 1987). For brevity we refer to the newly synthesized nickel and its decay product cobalt as Ni-Co. We refer to the inner region of the ejecta where newly synthesized Ni-Co dominates the composition as the Ni-Co-Fe core. UV spectra allow us to investigate the newly synthesized Ni-Co abundances in the ejecta as functions of depth, and thus constrain Type Ia explosion models. The outward extents of the newly synthesized Ni-Co and the Ni-Co-Fe core are particularly important for determining the nature of the burning front propagation and of mixing (if this in fact occurs) in Type Ia explosions. Unfortunately, the complexity of the line blending in the UV region means that information about abundances cannot be extracted easily and detailed analysis is needed.

UV photometry is important in helping to determine, by means of UV light curves, the photometric evolution and bolometric luminosity of Type Ia supernovae. This photometry can be extracted from *HST* or *IUE* spectra and obtained directly from the *HST*'s FOC using broad-band filters. At very early and probably never-to-be-observed epochs, the UV may dominate the bolometric luminosity of Type Ia's. In the premaximum and near-maximum light epochs, the UV still contributes significantly to the bolometric luminosity, although it is less important than the optical (e.g., Leibundgut et al. 1991). In the period from ~14 days before to ~340 days after maximum light, optical emission dominates the bolometric luminosity (Leibundgut 1988; Leibundgut et al. 1991; Spyromilio et al. 1992a). (We take the optical to comprise the wavelength range ~3500–10000 Å.)

Figure 1 displays our first two *HST* FOS spectra of SN 1992A. These spectra were taken using a 4″.3 × 4″.3 aperture. The spectra have not been smoothed but have been corrected for

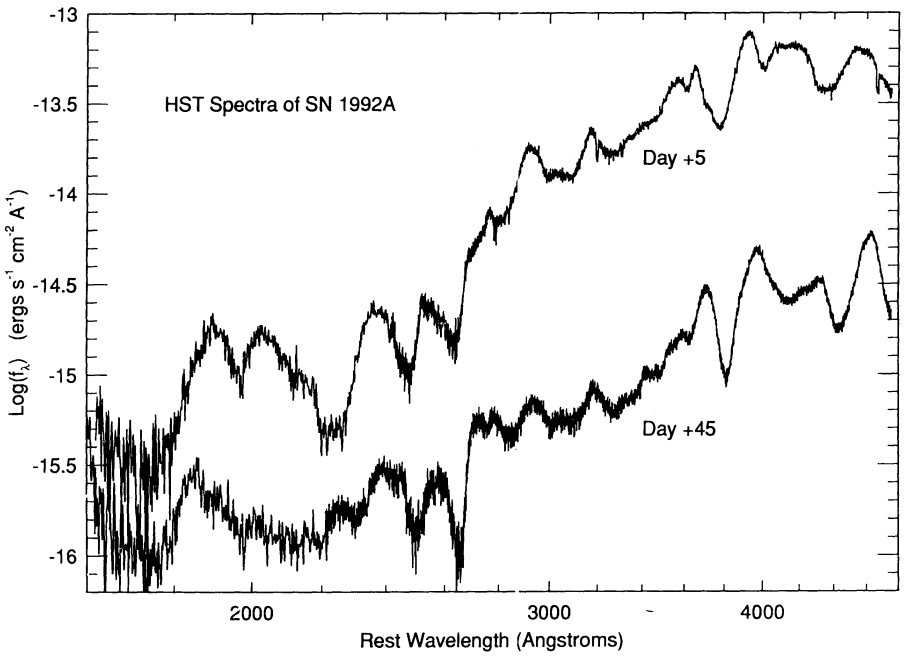

FIG. 1.—*HST* FOS spectra of SN 1992A. The spectra are labeled by their epochs relative to maximum light. They have not been smoothed. The spectra are the first *HST* spectra of a Type Ia supernova and the first Type Ia spectra where the region blueward of ~2650 Å has been observed with good signal-to-noise ratio. The rise in the spectra in the blueward direction near 1600 Å is an artifact of the FOS observations.

the heliocentric velocity 1809 km s^{-1} of NGC 1380. (All other observed spectra shown in this paper [except for the GHRS spectrum shown in Fig. 2 in § 2] have also been corrected for the heliocentric velocities of the parent galaxies. The heliocentric velocities have been taken from Tully 1988.) The UV regions blueward of ~2650 Å have never been adequately observed before for a Type Ia supernova, and their unveiling is one of the most important parts of this paper. When heavily smoothed, the near-maximum *IUE* spectra of the typical Type Ia SN 1981B blueward of ~2650 Å (e.g., Benvenuti et al. 1982) are consistent with the day +5 *HST* SN 1992A spectrum. Most *IUE* observations blueward of ~2650 Å of other Type Ia's (Benvenuti et al. 1982; Panagia & Gilmozzi 1991, Fig. 1) are of very poor quality and contain little significant information.

SN 1992A appears in most respects to be a typical Type Ia, so there is no reason to believe that SN 1992A's behavior in the region blueward of ~2650 Å is exceptional. The most striking aspect of this region is the appearance of absorptions centered at about 1980, 2240, 2480, and 2630 Å in the first *HST* spectrum and at about 2500 and 2650 Å in the second *HST* spectrum. As we will show, these absorptions are P Cygni absorptions formed in the expanding supernova atmosphere (see §§ 6.2 and 6.4). The rise in the spectra in the blueward direction near 1600 Å is an artifact of the FOS observations.

The SN 1992A spectra in Figure 1 (and everywhere else in this paper) have not been corrected for extinction. The foreground Galactic $E(B-V)$ of NGC 1380 is 0.00 mag (Burstein & Heiles 1984). The blue continuum shown by early spectra and the lack of interstellar Na I D lines in the spectra suggest that the extinction in NGC 1380 is small (Suntzeff & Roth 1992; see also Spyromilio & Bailey 1993). Furthermore, we have compared the premaximum optical spectra of SN 1990N, SN 1991T, and SN 1992A corrected for parent galaxy redshift and foreground Galactic extinction (which is nonzero only in the case of SN 1990N; Burstein & Heiles 1984), and they are very similar in continuum shape. We infer that optical continuum formation in these three Type Ia's is similar, and the parent galaxy extinction to all three is low. Based on this comparison, we estimate that the parent galaxy $E(B-V) \lesssim 0.1$ mag for all them. SN 1991T did show significant interstellar Na I D lines (Filippenko et al. 1992a; Ruiz-Lapuente 1992; Ruiz-Lapuente et al. 1992; Phillips et al. 1992), and so there must have been at least some small parent galaxy extinction toward this supernova. For SN 1990N (for which no strong interstellar lines were observed; Leibundgut et al. 1991) and SN 1992A, the best estimate for the parent galaxy extinctions is zero.

In § 2 of this paper we discuss interstellar lines in the day +5 high-resolution GHRS spectrum of SN 1992A. In § 3 we present the UV light curves of SN 1992A obtained from our *HST* FOS and FOC observations and *IUE* observations. We have done a synthetic spectrum analysis of the SN 1992A spectra through day +47. Section 4 introduces the assumptions and procedure of the synthetic spectrum analysis. In § 5 we discuss Type Ia models and the particular Type Ia model, a slightly modified version of the delayed-detonation model DD4 of Woosley (1991), that we have used for the analysis. In § 6 we present the synthetic spectrum analysis itself. A brief discussion of the 2650–3300 Å region of Type Ia spectra is given in § 7. The implications for Type Ia models of the O I λ7773 line in Type Ia spectra are discussed in § 8. In § 9 we discuss the question of the spherical symmetry of Type Ia supernovae in light of the spectropolarimetric observations of SN 1992A reported by Spyromilio & Bailey (1993). Section 10 presents a concluding discussion. (An observational paper reporting other light curves and more spectra for SN 1992A is in preparation; Suntzeff et al. 1993.)

Before ending this introduction, there are a few further points we would like to discuss. In this paper we define a typical Type Ia supernova to be one with spectra similar to those of the well-observed Type Ia's SN 1972E (Kirshner et al. 1973a), SN 1981B (Branch et al. 1983), and SN 1989B (Barbon et al. 1990; Wells et al. 1993) and with light curves that follow closely the Type Ia template light curves of Leibundgut (1988, 1993). We have classified SN 1992A as a typical Type Ia. SN 1992A seems to deviate from typicality only in that its light curves from later than 50 days after maximum light declined somewhat faster than the template light curves (Suntzeff et al. 1993). Type Ia's that are clearly atypical are SN 1984A (Wegner & McMahan 1987; Branch 1987; Barbon, Iijima, & Rosino 1989), SN 1986G (Phillips et al. 1987), SN 1991T (Filippenko et al. 1992a; Ruiz-Lapuente 1992; Ruiz-Lapuente et al. 1992; Phillips et al. 1992; Jeffery et al. 1992; hereafter JLK), and SN 1991bg (Filippenko 1992b; Leibundgut et al. 1993). At present we are uncertain whether SN 1990N (Leibundgut et al. 1991; JLK; Mazzali et al. 1993) should be classified as typical or atypical (see the discussion in § 7).

Observations of Type Ia supernovae show no evidence for rise times from explosion to maximum light that are shorter than ~ 15 days, and Cadonau, Sandage, & Tammann (1985) find 20 days as an upper limit on the Type Ia rise time. In the particular case of SN 1990N, the rise time is known to be longer than 17.5 days (Leibundgut et al. 1991). In this paper we assume that the Type Ia rise time is 20 days.

We have considered the possibility of parent galaxy UV background contaminating our *HST* observations of SN 1992A. A preliminary examination of our November 5 *HST* spectrum shows that any parent galaxy UV background is less than $\sim 5 \times 10^{-17}$ ergs cm^{-2} s^{-1} Å^{-1} at least in the $\sim$1900–3300 Å region and less than $\sim 5 \times 10^{-18}$ ergs cm^{-2} s^{-1} Å^{-1} in the $\sim$2000–2500 Å region. Therefore, there is no UV background contamination in our pre-November *HST* observations.

2. INTERSTELLAR LINES IN A HIGH-RESOLUTION GHRS SPECTRUM OF SN 1992A

Supernovae are bright point sources with intrinsic features that are very broad compared with interstellar lines. Thus supernovae are useful background sources for high-resolution spectroscopic studies of the interstellar medium in the Galaxy and in parent galaxies. Using the *IUE*, high-resolution spectra have been obtained from Type II supernovae SN 1980K (Pettini et al. 1982) and SN 1987A (de Boer et al. 1987; Dupree et al. 1987; Blades et al. 1988a, b) and Type Ia supernova SN 1990N (the observation is referred to by Panagia & Gilmozzi 1991). For SN 1992A we used the GHRS to observe the Mg II UV resonance absorption lines (rest wavelengths 2796 and 2803 Å; e.g., Wiese, Smith, & Miles 1969) from interstellar gas in the Galaxy and in NGC 1380. Integration for 3916.8 s at a resolution of 0.092 Å per diode on 1992 January 24 (i.e., on day +5) (see Table 1) provided the spectrum shown in Figure 2.

The only absorption lines detected have small wavelength shifts and are due to low-velocity gas in the Galaxy. The lines have equivalent widths $W_\lambda(2796) = 0.87$ Å and $W_\lambda(2803) = 0.84$ Å with uncertainties of $\sim$0.2–0.3 Å. These modest equivalent widths are consistent with the low absorption along the line of sight to SN 1992A which we argued for in § 1. No evidence for gas in NGC 1380 or for Galactic high-velocity clouds is present in the spectrum; there is a 2 σ upper limit of $\sim$30 mÅ on the equivalent widths of the lines due to the NGC 1380 interstellar medium or to Galactic high-velocity clouds. The 30 mÅ upper limit corresponds, for a reasonable Doppler param-

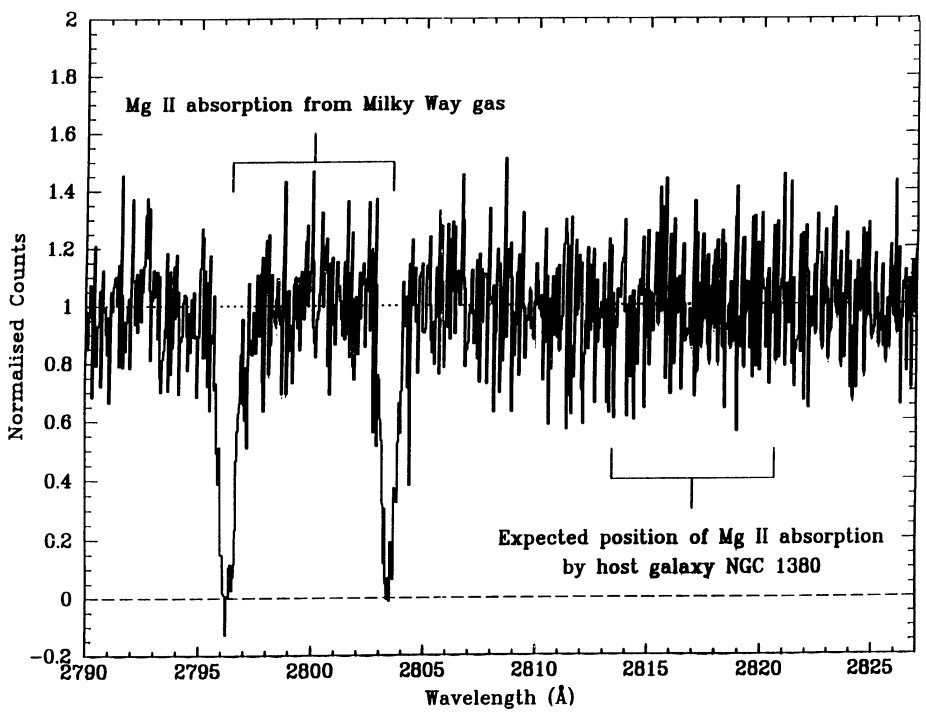

FIG. 2.—High-resolution *HST* GHRS spectrum of SN 1992A from 1992 January 24 (i.e., day +5). The spectrum has not been corrected for parent galaxy redshift.

eter $b \geq 4$ km s^{-1} (similar to what is seen in other observations of absorbing clouds), to a column density of ionized magnesium of $N(\text{Mg II}) < 10^{12}$ cm^{-2}. (The Doppler parameter b is $2^{1/2}$ times the standard deviation of a Gaussian fit to the velocity profile of a line; Strömgren 1948.) For NGC 1380 the Mg II lines would be redshifted by 1827 km s^{-1} and would be expected at the wavelengths marked in the Figure 2; no lines attributable to NGC 1380 are detected in the spectrum.

3. THE UV LIGHT CURVES OF SN 1992A FROM *HST* AND *IUE* OBSERVATIONS

A full reporting and examination of the SN 1992A photometry is beyond the scope of the present paper. Here we only report the UV photometry of SN 1992A obtained from our FOC, FOS, and *IUE* observations in F175W, F275W, and F342W bands defined for the FOC and the *F275W band which we define below. The photometry is based on the preliminary calibration provided with the initial SN 1992A data set. We present the photometry in the form of mean fluxes. For the FOC photometry, the supernova images were integrated from the center of the supernova to a radius of 2".42 (110 image pixels), except in the case of the 1992 April 5 (day +77) FOC F175W and F275W images, where the integration was cut off at a radius of ~2".22 because of the faintness of the images beyond that radius. The integrations to 2".42 include essentially the entire point-spread function of the supernova; the integrations to ~0".22 do not include the entire point-spread functions and thus require a correction (see below). To obtain mean fluxes from the FOS and *IUE* spectra, we convolved the spectra with the appropriate filter passbands (Paresce 1990, p. 21) using the CALCPHOT program of the SYNPHOT package from STSDAS. The convolution for a mean flux, $f_\lambda(P)$, from a spectroscopic flux, $f(\lambda)$, is given by the expression

$$f_\lambda(P) = \int_0^\infty P(\lambda) f_\lambda(\lambda) \lambda \, d\lambda \Big/ \int_0^\infty P(\lambda) \lambda \, d\lambda \,, \qquad (1)$$

where $P(\lambda)$ is the filter passband (Horne 1988). We did not correct the spectra used in the convolutions for parent galaxy redshift, so that the FOC and spectrum-derived photometry would be exactly comparable; correcting the spectra would in fact have had a negligible effect on the values of the spectrum-derived mean fluxes. For the focal ratio F/96 that we used for our FOC observations and spectrum convolutions, the F175W, F275W, and F342W filters have peak wavelengths of 1730, 2740, and 3400 Å and FWHMs of 714, 594, and 706 Å (Paresce 1990, pp. 16–18).

Figure 3*a* shows the light curves from the *HST* data alone. Maximum light is the origin of the time axis. From FOC observations we obtained F175W, F275W, and F342W mean fluxes for 1992 January 24 UT (day +5) and 1992 April 5 (day +77). FOS F175W, F275W, and F342W mean fluxes were obtained for 1992 January 24 UT (day +5) and 1992 March 4 (day +45). In obtaining the FOS F175W mean fluxes there were two problems. First, the spectra end at ~1600 Å, while the F175W passband remains finite down to 1200 Å. Second, there is the spurious rise in the spectra in the blueward direction near 1600 Å (see Fig. 1). To avoid complications due to this artifact, we cut the spectra off at 1700 Å. As a result, the FOS F175W mean fluxes are only lower limits on the real supernova F175W mean fluxes. As one can see, the day +5 FOS F175W mean flux is ~0.12 dex (i.e., ~25% in linear units) lower than the day +5 FOC F175W mean flux; we attribute this discrepancy to flux in the real supernova spectrum below 1700 Å. We assume that the day +45 FOS F175W mean flux is also too low by ~0.12 dex. If we had not cut off the spectra, the FOS F175W mean fluxes for day +5 and day +45 would have been ~0.025 dex and ~0.008 dex higher, respectively; clearly, the real flux not integrated due to the 1600 Å end of the spectra is much greater than the contribution from the spurious rise.

The FOC and FOS F275W and F342W mean fluxes for day +5 agree to within ~0.01 dex and ~0.04 dex, respectively; we

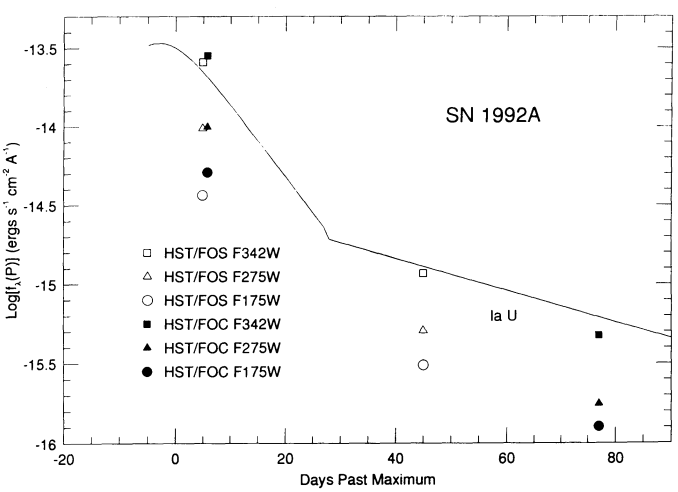

FIG. 3*a*

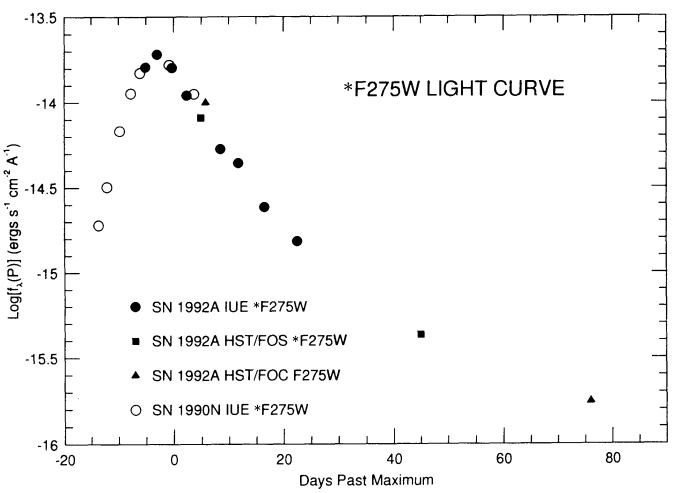

FIG. 3*b*

FIG. 3.—(*a*) F175W, F275W, and F342W light curves of SN 1992A from the *HST* observations. The solid curve is the Type Ia template *U* light curve of Leibundgut (1988, 1993); this light curve has been fitted to the F342W mean fluxes. The uncertainties in the mean fluxes and the template *U* light curve are discussed in the text. (*b*) Type Ia template *F275W light curve constructed from SN 1992A and SN 1990N observations. The uncertainty in the mean fluxes is discussed in the text.

conclude that the uncertainty in these mean fluxes is $\lesssim 0.04$ dex. We assume that the uncertainty in the day +5 FOC F175W and day +45 FOS F275W and F342W mean fluxes are also $\lesssim 0.04$ dex.

On day +77, the FOC images were faint, and only for the F342W filter was a full point-spread function visible. As noted above, the F175W and F275W images became too faint to measure beyond 0".22. In order to obtain F175W and F275W mean fluxes for day +77, we assumed that the point-spread function was the same for all filters on that day; this is reasonable, since the point-spread function was almost the same for all three filters on day +5. The day +77 point-spread function was obtained from the F342W image. The F175W and F275W mean fluxes were then obtained by dividing the integral of the flux to radius 0".22 obtained from the F175W and F275W images by the integral of the normalized point-spread function to the same radius. We estimate the uncertainty in all three day +77 mean fluxes to be at least ~ 0.05 dex.

The F342W passband strongly overlaps with the *U* passband, and thus for comparison we have fitted the Type Ia template *U* light curve (Leibundgut 1988, 1993) to the F342W mean fluxes. Within the uncertainty, the F342W and *U* light curves marginally agree. (The uncertainty in the template *U* light curve is ~ 0.1 dex.) The template *U* light curve also marginally agrees within the uncertainties with the F175W and F275W light curves. Thus, the overall UV flux behavior with time seems relatively constant with wavelength. The F175W, F275W, and F342W light curves decrease slightly faster than the Type Ia template *B* curve in the period ~ 40–80 days after maximum light.

The useful *IUE* wavelength range for Type Ia supernovae (~ 2650–3300 Å) prevents extracting F175W and F342W mean fluxes from *IUE* spectra. Even for the F275W filter, the useful *IUE* wavelength range for Type Ia's is actually a bit too narrow. On the blue side of the passband there is no difficulty, since Type Ia flux is very low and makes no significant contribution to the filter mean flux (see Fig. 1). On the red side of the passband, however, Type Ia flux is generally rising toward a maximum in the optical, and the passband, although decreasing rapidly, does not fall to zero until $\gtrsim 6000$ Å. For days with optical spectra complementing the *IUE* spectra, the missing flux from the red side of the passband could be estimated by using the optical spectrum in the convolution also. However, it is inconvenient to be unable to use the *IUE* spectra alone to obtain mean fluxes. Therefore, we have defined *F275W to be the passband of a filter that is exactly like the F275W filter, except that the *F275W filter cuts off at ~ 3400 Å. We impose the cutoff by putting a zero flux point at the red end of an *IUE* spectrum. (We should note that if a spectrum does not cover the whole of a passband range, then the CALCPHOT program does a 1 point constant extrapolation from the end values of the spectrum in order to achieve this coverage. Since the *IUE* spectra tend to be very noisy at the ends, the CALCPHOT extrapolation can result in a significant error if the endpoints are inaccurately very high or very low.) The exact wavelength of the cutoff of the *F275W filter is not important; the *IUE* spectrum is rather inaccurate in the ~ 3300–3400 Å region, but the contribution of this region is quite small. From our two FOS spectra, we find that *F275W mean fluxes are ~ 0.1 dex (or $\sim 20\%$ in linear units) lower than F275W mean fluxes; this result is likely to be fairly general.

In Figure 3*b* we present a Type Ia *F275W light curve constructed using the *IUE* and *HST* observations of SN 1992A and the *IUE* observations of SN 1990N. The *IUE* points have an uncertainty of ~ 0.04 dex. The SN 1990N *F275W mean fluxes were needed to complete the rising phase of the light curve; these mean fluxes were shifted vertically to fit the curve defined by the SN 1992A *F275W mean fluxes in the time interval of overlap between the two sets of fluxes. *IUE* spectra available from other Type Ia supernovae have poorer time coverage and would not extend our *F275W light curve; we intend to investigate the *F275W mean fluxes of these spectra in future work. We include in Figure 3*b* the FOC F275W mean fluxes. The day +5 FOC F275W mean flux is, as expected, ~ 0.1 dex above the curve defined by the *F275W mean fluxes. The day +77 FOC F275W mean flux must stand in for the *F275W mean flux, which is unavailable.

Our *F275W light curve shows a fairly detailed view of the UV evolution of a Type Ia supernova from 14 days before maximum light to 22 days after. The two points from after day +22 sketch the later *F275W light-curve behavior. For the present, we will consider this light curve as the typical Type Ia template *F275W light curve. It should be noted that SN 1990N may not have been a typical Type Ia, particularly in the UV (see § 7); nevertheless, SN 1990N data are indispensable since the early *IUE* time coverage of SN 1990N is unique. In Table 3 we present the light curve in terms of mean fluxes and in terms of magnitudes with maximum light set to 0 mag. In the magnitude form the light curve is immediately comparable to the template light curves of Leibundgut (1988, 1993). Our data suggest that the *F275W maximum is at day −3; this value has an uncertainty of at least a day. The *F275W light curve is similar to the template *U* light curve of Leibundgut (1988, 1993) (which also has its maximum on day −3), but is probably not quite consistent with this template light curve. The *F275W light curve seems to decline a bit faster from its maximum. It should be noted that the template *U* light curve does not extend earlier than day −5 (see Fig. 3*a*).

One special use of the template *F275W light curve might be in the study of Type Ia supernovae at high redshifts. It may be possible to use such distant Type Ia's for the determination of the deceleration parameter (e.g., Kirshner 1989; Perlmutter et al. 1991). At redshift of 0.6, for example, the intrinsic *F275W region of a Type Ia would be shifted by ~ 1750 Å and would be closely overlapping the *B* band. Thus *B*-band observations of the Type Ia's at redshift 0.6 could be compared with the *F275W light curve.

In future work we intend to investigate further the UV photometry of Type Ia supernovae. Because nearly all of the UV data available bluer than the *U* band are *IUE* spectra, most of our study will concentrate on photometry from the region covered by the *F275W band. Among other things, we hope to improve and extend our template *F275W light curve.

4. ASSUMPTIONS AND PROCEDURES OF THIS SYNTHETIC SPECTRUM ANALYSIS

The synthetic spectrum analysis of Type Ia spectra consists in calculating the radiative transfer through a Type Ia model and adjusting the model parameters to fit an observed Type Ia spectrum. The quality of the fits achieved and the values of the fit-giving parameters provide information about the observed Type Ia and allow a judgment to be made about the adequacy of the Type Ia model.

TABLE 3

THE TYPE Ia TEMPLATE *F275W LIGHT CURVE

Number	Epoch Relative to Maximum Light (day)	*F275W Mean Flux (10^{-15} ergs s^{-1} cm^{-2} $Å^{-1}$)	*F275W Magnitude (mag)
1.....	−13.68	1.91	2.27
2.....	−12.11	3.18	1.71
3.....	−9.77	6.78	0.89
4.....	−7.77	11.3	0.34
5.....	−6.09	14.9	0.04
6.....	−5.11	16.1	−0.05
7.....	−2.98	19.1	−0.23
8.....	−0.77	16.6	−0.08
9.....	−0.26	16.0	−0.04
10.....	0.00	15.4	0.00
11.....	2.37	11.0	0.37
12.....	3.66	11.2	0.35
13.....	4.94	8.14	0.69
14.....	8.47	5.34	1.15
15.....	11.71	4.40	1.36
16.....	16.47	2.43	2.01
17.....	22.46	1.53	2.51
18.....	45	0.43	3.89
19.....	77	0.176	4.86

NOTE.—Maximum light is taken to have zero magnitude just as for the template light curves of Leibundgut 1988, 1993. We have interpolated a day +0 entry. If the light-curve data are considered only as light-curve data for SN 1992A and SN 1990N, then the uncertainty in the mean fluxes is ~10% and the uncertainty in the magnitudes is ~0.1 mag. The uncertainties in the light-curve data considered as Type Ia template light-curve data require more Type Ia observations for determination.

For our calculations we have adopted a Type Ia model consistent with the standard Type Ia picture (see, e.g., Wheeler & Harkness 1990). In this picture, a Type Ia supernova is a C-O white dwarf of near the Chandrasekhar mass that has exploded due to a thermonuclear runaway leading to a deflagration or to a deflagration combined with a detonation. The white dwarf is totally disrupted and no remnant is left. The ejecta is all metal, is spherically symmetric, and passes into homologous expansion a few tens of seconds after the explosion. Because the expansion is homologous, all materially defined lengths in the ejecta scale linearly with time, and the radial velocities of the ejecta form a convenient comoving coordinate system. Our adopted Type Ia model is described in detail in § 5.

Our radiative transfer procedure uses a fitted temperature profile and assumes LTE for the calculation of atomic occupation numbers. We begin using a gray temperature profile similar to that used by JLK, but we allow ourselves the freedom to adjust it by hand. The temperature profiles that we used for our final fits are shown in § 6.

Because we are not doing a detailed ab initio calculation for the temperature and the atomic conditions, we have no information on these quantities at great depth. Thus, we assume an inner boundary that radiates like a blackbody (in the comoving frame) at the innermost temperature of the fitted temperature profile. At some point as one moves outward in the atmosphere, the LTE approximation becomes very poor. A crude approximation that we have adopted is to impose an outer boundary velocity on the radiative transfer calculation. Above this outer boundary velocity, we assume that non-LTE (NLTE) effects have rendered the ejecta effectively transparent. Usually, the outer boundary velocity was chosen to be the velocity corresponding to the blue edge of the broadest P Cygni absorption appearing in a spectrum. Such a blue edge marks the outermost point in the ejecta that we can clearly identify from the spectrum.

The LTE approximation allows us to calculate plausible line opacities. However, using LTE line source functions (i.e., line source functions that are the Planck function evaluated at the local temperature) is a poor approximation for supernovae, where the line source functions are probably much closer to pure scattering source functions (e.g., Wagoner, Perez, & Vasu 1991). We found, however, that pure scattering source functions did not give a large enough UV flux deficiency for Type Ia supernovae (see below). Therefore, we have adopted a two-level–atom source function for the lines that is a combination of the pure scattering and LTE source functions (see, e.g., Mihalas 1978, p. 337). The parameter that controls the contribution of the pure scattering and LTE source functions is ϵ: for $\epsilon = 0$ there is pure scattering; for $\epsilon = 1$ there is a pure LTE source function. We treated ϵ as an adjustable parameter. There is some trade-off between ϵ and temperature that prevents finding a unique set of values for the parameters. Usually we used a global ϵ-value for all lines and velocities.

The radiative transfer in both lines and continuum was calculated using the relativistic Sobolev method (Hutsemékers & Surdej 1990; Jeffery 1993). The continuum radiative transfer with the Sobolev method was done using the discretized continuous opacity approximation (Jeffery 1988, 1989, 1991b). All relevant lines from the Kurucz line data files, which contain $\sim 5 \times 10^5$ lines (Kurucz 1991), were included in the radiative transfer calculations. The only continuous opacities included were the quasi-continuous expansion opacity and electron scattering opacity. The expansion opacity is caused by the strong overlapping of lines due to the macroscopic velocity field; the overlapping makes a continuous opacity out of the collective effect of the line opacities (Karp et al. 1977). The

expansion opacity is important in wavelength regions of high line density. We do not consider bound-free or free-free opacity as part of the expansion opacity. The expansion opacity arises naturally in our calculations because of our use of all the relevant lines. The electron scattering opacity was calculated from our temperature profiles and the density profile of our adopted model (see § 5) using LTE. Pure scattering source functions used were for the electron scattering opacity.

For reference, Table 4 displays the line data for the atomic multiplets that we mention in the discussion of the synthetic spectrum analysis. We will refer to each multiplet using its mean wavelength: e.g., Fe II λ2346 for the first Fe II multiplet appearing in Table 4. The lines represented in Table 4 are only a small subset of the lines used in the calculations. Most of the lines used are very weak; their cumulative effect, however, is important. The well-known UV flux deficiency of Type Ia spectra relative to blackbody fits to the optical is a consequence of a large UV expansion opacity (Wheeler et al. 1986; Harkness 1991b) to which many lines too weak to be identified individually contribute. The UV flux deficiency is well reproduced in our synthetic spectra (see § 6). Moreover, lines strong enough to give rise to P Cygni profiles are often modulated by line blending due to weak lines.

In this paper we define the photosphere to be at a continuum optical depth of $\frac{2}{3}$ and the electron scattering photosphere to be at an electron scattering optical depth of $\frac{2}{3}$. In the optical region of Type Ia supernovae in the premaximum and near-maximum epochs, the continuous opacity is almost entirely due to electron scattering opacity and thus the photosphere and electron scattering photosphere can be assumed to be nearly the same. The UV expansion opacity provides the UV region with a photosphere that is larger in radius than the electron scattering photosphere.

We do not attempt to determine the synthetic spectrum absolute flux. Instead we scale a synthetic spectrum so that it has the same integrated flux as an observed spectrum over a specified wavelength range. Since the observed optical spectrum is most easily fitted, it is natural to use integrated fluxes from some part of the optical region. Usually, we integrate over a large subrange of range $\sim$4000–6500 Å, so that the weaker synthetic optical lines of silicon, sulfur, and iron are fixed at the right overall flux level.

Because our radiative transfer calculations are heavily parameterized and rely on LTE, the model parameters we determine and our judgment about the adequacy of a Type Ia model are suggestive, not definitive. If some set of parameters for a model yield a reasonable fit, then the model is viable. Ruling out models is more difficult, since the deficiencies of the model can be attributed to the deficiencies of the parameterized LTE calculation. Nevertheless, guidance to a correct model can be obtained from the conclusions of a parameterized LTE analysis. For example, important evidence can be obtained from the analysis of the P Cygni line due to the Si II λ6355 multiplet. This line is much too strong in Type Ia supernovae to be due to solar silicon abundance for any plausible Type Ia temperature profile, given that LTE holds. The LTE analysis predicts that silicon abundance needs to be $\sim$2–3 dex larger than solar; in the exploding white dwarf picture for Type Ia's, such a high abundance implies that most of the silicon has been newly synthesized in the explosion. Since NLTE calculations (Branch et al. 1991) confirm the need for silicon abundances $\sim$2–3 dex greater than solar in fitting the Si II λ6355 multiplet absorption of Type Ia's, we conclude that the parameterized LTE analysis can detect the need for newly synthesized silicon.

As a final remark, it must be noted that the definitive analyses of Type Ia spectra require time-dependent, self-consistent, NLTE calculations. Physically correct calculations of this sort are formidable undertakings. However, various workers are making progress toward this goal (Harkness 1991a, b; Branch et al. 1991; Höflich, Khokhlov, & Müller 1991; Höflich, Müller, & Khokhlov 1992; Ruiz-Lapuente 1992; Ruiz-Lapuente et al. 1992; Mazzali et al. 1993; Eastman & Pinto 1993).

5. THE TYPE Ia MODEL

A favorite Type Ia model over the past few years has been the deflagration model W7 of Nomoto, Thielemann, & Yokoi (1984) and Thielemann, Nomoto, & Yokoi (1986). Model W7 or variations of it have been quite successful in reproducing the maximum and near-maximum light spectra of Type Ia supernovae (Branch et al. 1985, 1991; Harkness 1991a, b; Ruiz-Lapuente 1992; Mazzali et al. 1993). This suggests that there is something right about model W7. The burning front in model W7 quenched at $\sim$15,000 km s^{-1}. Above this velocity, the original W7 composition consists of only carbon and oxygen with a trace of neon; this composition is physically implausible. It is usual to take the composition of model W7 above the quenching point to be a C-O–solar composition with equal amounts of carbon and oxygen (i.e., a solar composition with all elements lighter than carbon turned into equal amounts of carbon and oxygen). There is now considerable evidence to show that the burning front in at least some Type Ia's must propagate farther out than $\sim$15,000 km s^{-1}.

The principal evidence for propagation beyond $\sim$15,000 km s^{-1} comes from the Si II λ6355 multiplet P Cygni line in Type Ia spectra. The blue edges of the Si II λ6355 absorptions in the earliest available spectra of SN 1984A (Wegner & McMahan 1987; Branch 1987; Barbon et al. 1989) and SN 1990N (Leibundgut et al. 1991; JLK) correspond to velocities of $\sim$25,000 km s^{-1}. In LTE with a C-O–solar composition, it seems impossible to produce Si II λ6355 multiplet absorption blue edges as "fast" as this. As we discussed in § 4, the Si II λ6355 multiplet in Type Ia supernovae is probably not strongly enhanced by NLTE effects, and thus we conclude that model W7 cannot be correct for SN 1984A and SN 1990N. Now SN 1984A was an atypical Type Ia; many important line features in SN 1984A were substantially more blueshifted than the same line features in almost all other Type Ia's when compared at similar epochs (Wegner & McMahan 1987; Branch 1987; Barbon et al. 1989, 1990). SN 1990N initially appeared to be a typical Type Ia, but it exhibited noticeable differences from those Type Ia's we clearly identify as typical (see § 7); its high-velocity Si II λ6355 blue edge came from a spectrum from 14 days before maximum light, an epoch at which no other Type Ia has been observed, and so provides no evidence for or against atypicality.

For SN 1992A, the case is less clear cut than for SN 1984A and SN 1990N for enhanced silicon abundance at velocities higher than $\sim$15,000 km s^{-1}. However, the blue edge of the Si II λ6355 multiplet from the day -7 SN 1992A spectrum (the earliest available) yields a velocity of $\sim$19,000 km s^{-1}. Test calculations with model W7 showed that no temperature profile we could engineer would make the synthetic Si II λ6355 absorption as broad as the observed Si II λ6355 absorption in

TABLE 4

MULTIPLETS AND LINES RELEVANT TO THE DISCUSSION OF THE SN 1992A SPECTRA

Ion	Multiplet			Strongest Line(s) of Multiplet		
	Mean λ (Å)	Mean E_L (eV)	log (gf)	λ (Å)	E_L (eV)	log (gf)
C I[a,b]	1931	1.264	−0.39	...	...	...
Cr II[c]	2060	0	0.368	2056	0	0.025
Ni II[a]	2182	1.193	0.847	2166	1.041	0.260
Ni II[a]	2235	1.137	0.981	2216	1.041	0.541
Ni II[a]	2286	1.758	0.423	2279	1.680	0.174
Ni II[a]	2305	1.776	0.557	2297	1.680	0.192
Ni II[a]	2309	1.152	0.725	2316	1.041	0.314
Fe II[c]	2346	0.057	0.651	2343	0	0.112
Fe II[a]	2357	0.287	0.147	2360	0.232	−0.367
Fe II[a]	2365	0.306	0.405	2348	0.232	−0.100
Fe II[c]	2395	0.053	1.093	2382	0	0.557
Fe II[a]	2571	1.034	0.484	2563	0.986	0.062
Fe II[c]	2608	0.047	0.950	2599	0	0.417
Fe II[a]	2741	1.025	0.737	2740	0.986	0.331
Fe II[a]	2749	1.036	0.875	2756	0.986	0.425
Mg II	2796	4.430	0.742	2978	4.434	0.742
Mg II[c]	2798	0	0.274	2796	0	0.098
				2803	0	−0.203
Mg II	2934	4.430	−0.079	2937	4.434	−0.255
Fe II[a]	2974	1.687	0.104	2985	1.671	−0.339
Cr II[a]	3128	2.458	0.903	3132	2.483	0.451
Fe II[a]	3188	1.681	−1.713	3196	1.671	−1.957
Fe II[a]	3212	1.689	−0.464	3228	1.671	−0.864
Cr II[a]	3387	2.467	0.215	3409	2.483	−0.038
Cr II[a]	3402	2.451	0.291	3423	2.455	−0.266
Co II	3430	2.234	−0.585	3502	2.203	−1.180
Co II	3530	2.737	−1.132	3508	2.779	−1.502
Co II	3593	2.216	−1.176	3621	2.203	−1.411
Co II	3594	2.703	−1.264	3606	2.681	−1.505
Ni II[a]	3624	3.053	−1.385	3769	3.104	−1.662
Ca II	3726	3.142	0.016	3737	3.151	−0.160
Co II	3746	3.096	−1.829	3755	3.086	−1.918
Si II	3858	6.859	−0.43	3856	6.859	−0.65
Ca II[c]	3945	0	0.318	3934	0	0.140
				3968	0	−0.162
Si II	4130	9.838	0.71	4130	9.839	0.462
Co II	4152	3.452	−1.493	4161	3.408	−1.828
Co II	4302	5.066	−1.728	4417	5.068	−2.264
Fe III[a]	4404	8.246	−1.824	4420	8.241	−2.218
Co II	4479	3.430	−2.284	4497	3.406	−2.539
Mg II	4481	8.864	0.978	4481	8.864	0.740
Fe II[a]	4555	2.828	−1.365	4549	2.828	−1.957
				4584	2.807	−1.802
Si III	4560	19.016	0.55	4553	19.016	0.290
Fe II[a]	4561	2.829	−1.731	4629	2.807	−2.306
Co II	4607	3.395	−1.905	4661	3.361	−2.205
Co II	4852	5.187	−2.338	4829	5.175	−2.532
Si II	5051	10.072	0.65	5056	10.074	0.42
Fe II[a]	5060	2.891	−0.931	4924	2.891	−1.559
				5018	2.891	−1.400
				5169	2.891	−1.303
Fe III[a]	5129	8.651	−1.570	5156	8.641	−2.018
S II	5208	15.068	0.51	5213	15.068	0.24
S II	5331	15.068	0.71	5321	15.068	0.46
S II	5468	13.639	0.86	5454	13.672	0.44
S II[a]	5612	13.696	0.47	5606	13.733	0.04
S II	5654	14.046	0.56	5640	14.067	0.33
Fe III	5876	18.509	0.979	5834	18.509	0.616
[Co III][c]	5894	0	−7.567	5890	0	−7.682
				5908	0	−8.202
Si II	5972	10.072	0.12	5979	10.074	−0.06
Si II	6355	8.121	0.401	6347	8.121	0.225
				6371	8.121	−0.074
S II	7628	14.261	−0.578	7590	14.234	−0.880
O I[a]	7773	9.146	0.664	7772	9.146	0.333
Si II	7850	12.525	0.73	7850	12.526	0.49
Mg II	7890	9.998	0.87	7896	9.999	0.65
Ca II[a]	8579	1.697	−0.143	8498	1.692	−1.315
				8542	1.700	−0.365
				8662	1.692	−0.62
Mg II	9226	8.655	0.438	9218	8.655	0.262
O I	9264	10.741	1.130	9266	10.741	0.69
Si II	9413	12.839	1.236	9413	12.839	0.980
Ca II	11873	6.468	0.48	11836	6.468	0.29

NOTE.—The atomic line data for the intermediate-mass elements are almost entirely taken from Wiese, Smith, & Glennon 1966 and Wiese et al. 1969. The atomic line data for the iron peak elements and a few of the intermediate-mass elements are taken from the Kurucz atomic data files (see Kurucz 1991 for a description), except for the [Co III] λ5894 data, which were provided by Pinto 1992. For uncertainties in the data, one should consult the original sources; we have usually quoted more digits than are significant for reasons of tabular consistency. The gf value of a multiplet is the sum of the gf values of the multiplet's lines. For the multiplets taken from Wiese et al. 1966, 1969, the mean quantities are determined as described by Wiese et al. 1966 (pp. viii, xi). For multiplets taken from the Kurucz data files, the mean wavelength and lower term energy are the gf-weighted means of the multiplet line wavelengths and lower level energies, respectively. The strongest multiplet lines were taken to be those with the largest gf values. Useful Grotrian diagrams for most of the ions cited in the table are given by Moore & Merrill 1968.

[a] The lower term of this multiplet is a metastable term.

[b] This multiplet has only one line.

[c] The lower term of this multiplet is the ground term.

the day −7 spectrum. We conclude that it is probable that the newly synthesized silicon extends out at least to ~19,000 km s^{-1} in SN 1992A. Since SN 1992A seems to be an entirely typical Type Ia, we tentatively conclude that model W7 cannot be adequate for most Type Ia's.

Recently, two new classes of Type Ia models, the delayed-detonation models (Khokhlov 1991a, b; Woosley 1991) and the late-detonation models (Yamaoka et al. 1992), have been proposed to address the need for fast newly synthesized elements. In both classes of models, the burning front is propagated by a deflagration wave (i.e., turbulent subsonic propagation) that turns into a detonation wave (supersonic propagation) at some specified mass coordinate. The deflagration wave causes a nonburning subsonic pressure front that expands ejecta ahead of deflagration wave. The preexpansion lowers the burning rates in the outer ejecta, and thus prevents the detonation wave when it turns on from producing only iron peak elements. (In pure detonation models, iron peak elements produced by the detonation wave dominate the composition everywhere in the ejecta. The observed presence of significant intermediate-mass elements in Type Ia ejecta rules out pure detonation models.) In delayed-detonation models, the detonation wave is turned on at a mass coordinate much less than 1 $M_\odot$. The composition produced by a delayed-detonation model can be made to be similar to that of model W7, but with the newly synthesized element layers stretched out to higher velocities. In the late-detonation models, the detonation turns on at a mass coordinate of $\gtrsim 1.1\ M_\odot$, which corresponds to a velocity of ~12,000 km s^{-1}. Below the turn-on mass coordinate, a late-detonation model can have a composition much like that of model W7; above, layers rich in iron peak and silicon peak elements can be produced that extend beyond ~30,000 km s^{-1}.

As we will show in § 8, the current versions of the late-detonation model can be ruled out as models for Type Ia supernovae. The delayed-detonation models, however, look promising. One such model, model DD4 of Woosley (1991), reproduces quite well the nebular epoch spectra of Type Ia's (Eastman & Pinto 1993; Pinto 1992). (The epoch when a Type Ia is completely nebular probably starts sometime after 100 days after explosion.) The DD4 composition also appeared adequate to account for most of the photospheric epoch spectra of SN 1992A. The fact that its newly synthesized silicon extends to ~25,000 km s^{-1} is particularly desirable. Therefore, we adopted model DD4 (with a small modification of the composition: see below) for the synthetic spectrum analysis we report in § 6.

The total mass and kinetic energy of model DD4 are 1.386 $M_\odot$ (i.e., nearly the Chandrasekhar mass) and 1.22×10^{51} ergs, respectively. In the homologous epoch, the density profile shape is a constant with time, and the density at each velocity decreases as the inverse third power of time. The version of model DD4 we have is specified as being at 1020 s after the explosion; the model ejecta is in homologous expansion by this epoch (see § 4). Using the DD4 density profile at 1020 s, the condition of homologous expansion, and our assumption of a 20 day rise time for Type Ia's we have calculated the DD4 density profiles for those observed epochs of SN 1992A for which we wished to do synthetic spectrum calculations.

The homologous epoch density profile of model DD4 is very nearly an inverse exponential profile with e-folding velocity 2800 km s^{-1} from the center to the model cutoff at 28,340 km s^{-1}. We extrapolate exponentially the density profile from the last two model points when ejecta at velocities higher than 28,340 km s^{-1} are needed.

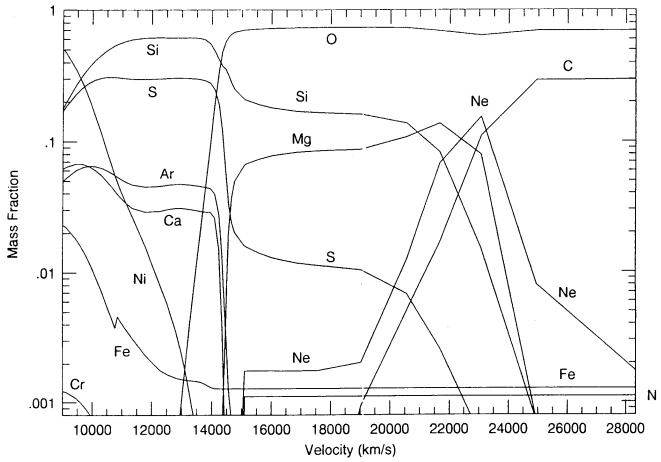

FIG. 4.—Modified DD4 composition at 1020 s, by which time the ejecta motion has become homologous expansion. We show only the velocity range 9000–28,340 km s^{-1}. Below 9000 km s^{-1} the composition is dominated by ^{56}Ni; this region is the Ni-Co-Fe core. The composition above 28,340 km s^{-1} is extrapolated from the composition at 28,340 km s^{-1}. After the explosion, the composition changes because of the decay of the explosion-synthesized ^{56}Ni to ^{56}Co, which in turn decays to ^{56}Fe.

The (modified) DD4 composition, except for the Ni-Co-Fe core, that we have used for the analysis is displayed in Figure 4. This is the composition that the ejecta would have a few tens of seconds after the explosion when homologous expansion had set in. In model DD4, as in model W7, the boundary of the Ni-Co-Fe core is at ~9000 km s^{-1}. We extrapolate the composition from the last model point when ejecta at velocities higher than 28,340 km s^{-1} are needed.

The model DD4 placement of the Ni-Co-Fe core boundary at ~9000 km s^{-1} agrees with the evidence from Type Ia line velocities. The line velocity of a P Cygni line is the velocity corresponding to the blueshift of the minimum of the P Cygni absorption. The line velocity of an unblended P Cygni line cannot usually be any smaller than the (radial) velocity of the slowest moving matter that can give rise to that line. The line velocities for intermediate-mass elements in Type Ia's are almost never significantly below ~9000 km s^{-1}. Thus, it is reasonable to suggest for typical Type Ia's that there is no significant amount of intermediate-mass elements below ~9000 km s^{-1} and that ~9000 km s^{-1} is the Ni-Co-Fe core boundary velocity.

Smaller line velocities than ~9000 km s^{-1} are attributed to the Si II λ6355 multiplet in the atypical Type Ia's SN 1986G and SN 1991bg (Leibundgut et al. 1993) and to the Mg II λ4481 multiplet in several Type Ia's (Barbon et al. 1990; Benetti & Barbon 1991). The slow Si II λ6355 multiplet line velocities may be caused by line blending and perhaps by misidentification, since these line velocities come from later than 10 days after maximum light when the Fe II lines are becoming strong in the spectral region where the Si II λ6355 multiplet line would form. On the other hand, it may be that these atypical Type Ia's have smaller Ni-Co-Fe core boundary velocities than other Type Ia's. Further investigation of the Ni-Co-Fe core boundary in SN 1986G and SN 1991bg is needed. The slow Mg II λ4481 multiplet line velocities are probably due to misidentification,

since we find that Fe II and Fe III lines are responsible for the absorption attributed to the Mg II λ4481 multiplet in the period after ~ 5 days after maximum when the slow line velocities were measured (see, e.g., §§ 6.2 and 6.3). Because of these considerations, we believe that the ~ 9000 km s^{-1} Ni-Co-Fe core boundary velocity estimate is not undermined by the reported slow intermediate-mass element line velocities.

Model DD4 was calculated from a pure C-O white dwarf (carbon and oxygen mass fractions 0.3 and 0.7, respectively). Since elements other than carbon and oxygen must be present in real C-O white dwarfs, a modification to the DD4 composition is needed. We made the simple assumption that the nitrogen and all elements from fluorine to germanium had solar abundances everywhere in the white dwarf before the burning started. Therefore, we added a solar abundance of all these elements to the DD4 composition in those regions where the nuclear burning was unlikely to have affected them. For example, we only add the solar neon abundance in the outer layers where it is unlikely that neon burning would have occurred. The step-function–like rise in abundances of some light elements at $\sim 15{,}000$ km s^{-1} results from our abundance adding procedure. The burning front in model DD4 had essentially stopped by the last model point. Because of our addition of solar abundances, the composition at the last model point is a C-O-solar composition with carbon and oxygen in the ratio 3 to 7 by mass. (The solar abundances used in this paper are the solar system abundances of Anders & Grevesse 1989.)

Model DD4 was calculated with a limited burning network including only the elements hydrogen, helium, carbon, nitrogen, oxygen, neon, magnesium, silicon, sulfur, argon, calcium, titanium, chromium, iron, and ^{56}Ni. For our synthetic spectrum calculations, the ^{56}Ni was converted into the proper amounts of nickel, cobalt, and iron for the epoch of the spectrum being analyzed. The elements left out of the DD4 burning network, with the exception of manganese, seem to be relatively unimportant for Type Ia spectrum formation. Because of our abundance adding procedure, small amounts of these elements are present in our modified DD4 composition.

6. THE SYNTHETIC SPECTRUM ANALYSIS OF THE EARLY SN 1992A SPECTRA

Figure 5 displays most of our SN 1992A spectra (see also Table 2); overlapping regions and five of the *IUE* spectra have been omitted for clarity; some spectra have been combined to improve the signal-to-noise ratio or wavelength coverage. The narrow wavelength range UV spectra are from the *IUE*, the broader wavelength range UV spectra are our *HST* spectra, and the optical spectra are from CTIO. The UV spectra have been binned in 10 Å intervals in order to reduce noise. Only the day $-7/6$ spectrum (a combination of the day -7 and day -6 spectra) has the correct flux scale; all the other spectra have been vertically displaced for clarity. The day $-7/6$ combined spectrum was created because the two day -7 spectra had low photometric accuracy, but one of them extended farther to the red than the fairly photometrically accurate day -6 spectrum, which cut off at 7600 Å. The day -7 and day -6 spectra agree in the region of overlap; therefore, only the scale of the 7600–8350 Å region in the day $-7/6$ combined spectrum is suspect. The *IUE* and optical spectra for day -5 do not connect to each other. The day $+5$ and day $+45$ *HST* spectra have been complemented with optical CTIO spectra taken on day $+6$ and day $+47$, respectively; the *HST* and optical spectra are in their observed relative locations. In the regions (not shown in Fig. 5) where the *HST* and optical spectra overlap, they are in good agreement. We will refer to the combined *HST* and optical spectra as the day $+5/6$ and day $+45/47$ spectra.

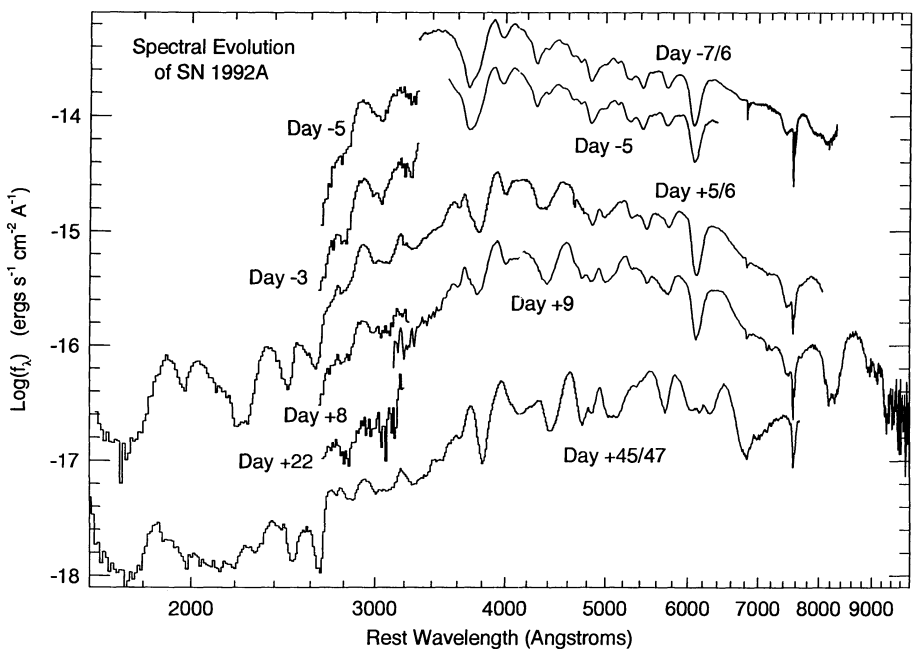

FIG. 5.—Sample of SN 1992A spectra showing the early spectral evolution. The spectra are labeled by epoch relative to maximum light. The narrow wavelength range UV spectra are from the *IUE*, the broader wavelength range UV spectra are our *HST* spectra, and the optical spectra are from CTIO. The UV spectra have been binned in 10 Å intervals in order to reduce noise. Only the day $-7/6$ spectrum is in its correct location; all the other spectra have been vertically displaced for clarity.

The spectrum of SN 1992A changed slowly in the period between day −7/6 and day +9. The most noticeable change is a decrease in the blueshifts of the P Cygni absorptions. This decrease is due to the expansion which causes the photosphere (above which the lines form) and the regions of strong line opacity (in which the lines form) to recede into the ejecta. The electron scattering photosphere should recede to ∼9000 km s^{-1} at about 20 days after the explosion and should reach the center of the ejecta at about 60 days after the explosion (JLK). As with the spectra of most other Type Ia's, there is no evidence in the SN 1992A spectra for intermediate-mass elements at velocities slower than ∼9000 km s^{-1}, the probable typical Type Ia Ni-Co-Fe core boundary velocity (see § 5).

The SN 1992A spectrum does change dramatically in the optical region in going from day +5/6 to day +45/47, whereas the ∼2400–4000 Å region continues to be fairly constant. This slow evolution of the ∼2400–4000 Å region probably occurs because this region is formed by lines with very large opacities. A spectrum tends to respond much more weakly than linearly to line opacity when line opacity is large. Thus, even relatively large changes in the large line opacities in the ∼ 2400–4000 Å region due to falling temperature (see below) and density due to expansion probably have only a relatively small effect on the spectrum. The optical lines of Si II, S II, Fe III, and probably Mg II that are present in the premaximum and near-maximum SN 1992A spectra (see below) and are characteristic of the premaximum and near-maximum spectra of Type Ia's have smaller opacities than the strong lines in the ∼2400–4000 Å region, and thus they evolve more obviously with falling temperature and density. Because of the falling temperatures, these optical lines have probably disappeared altogether by day +45/47 in SN 1992A (see § 6.4) and other Type Ia's.

Fitting synthetic spectra at widely separated epochs of SN 1992A can give model DD4 an extensive test. Therefore, we have calculated synthetic spectra for the day −7/6 optical spectrum combined with the *IUE* spectrum from day −5 (i.e., the day −7/6/5 spectrum), the day +5/6 *HST*/optical spectrum, the day +9 optical spectrum combined with the *IUE* spectrum from day +8 (i.e., the day +8/9 spectrum), and the day +45/47 *HST*/optical spectrum. The spectra used to make up the combined spectra are in their observed locations; no rescaling has been done. Because the epochs of the spectra we have combined are close, we expect that no great error has been introduced by the combination. The worst case is probably the earliest combined spectrum, since SN 1992A was evolving rapidly when the component spectra were taken. However, from extrapolation, the day −5 *IUE* spectrum is expected to be at most about 0.1 dex higher than the actual day −6 UV spectrum.

In the following subsections we present and discuss our synthetic spectrum fits. Figure 6 displays the temperature profiles that we arrived at for these fits. These profiles are consistent with the obvious notion that the temperatures at any fixed point in the ejecta above the Ni-Co-Fe core should fall with time. Empirically it is well known that the color temperature of Type Ia's falls significantly in the period from maximum light until ∼30 days after maximum light (Kirshner et al. 1973b; Branch et al. 1983). As mentioned in § 4, there is a trade-off between ϵ and temperature, and this causes an uncertainty of at least 1000 K in temperature at every velocity point in our calculations. A 1000 K temperature change can have a considerable effect on the spectrum formation, so an uncertainty of 1000 K is not negligible.

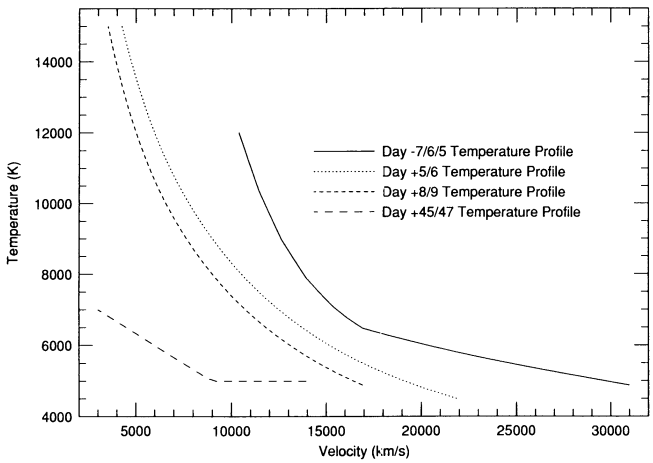

FIG. 6.—Temperature profiles used for the synthetic spectrum calculations

In the figures displaying the observed and synthetic spectra (see below), we have labeled the observed absorptions with the multiplets, and in some cases the lines, that we have identified as major contributors to those absorptions. The inner boundary synthetic spectra are also shown in these figures in order to illustrate the flux reduction caused by absorption and backscattering to the inner boundary in the model atmospheres. Since inner boundary blackbody emission is calculated in the comoving frame, the inner boundary synthetic spectra are not quite blackbody curves at inner boundary temperature. The difference from blackbody curves is less than 15% for the inner boundary velocities we consider when the wavelength is greater than ∼3000 Å or the inner boundary temperature is greater than ∼10,000 K. When the wavelength is less than 3000 Å and the inner boundary temperature less than 10,000 K, the difference can get much larger than 15%: e.g., for wavelength 1500 Å, inner boundary temperature 5000 K, and inner boundary velocity 13,000 km s^{-1}, the difference is ∼50%.

6.1. *The Day −7/6/5 Spectrum*

Figure 7 shows the observed day −7/6/5 spectrum and the synthetic spectrum fit. For the synthetic spectrum fit, the temperature profile shown in Figure 6 was used, ϵ was set to 0.1, and the inner and outer boundary velocities were 10,400 and 31,000 km s^{-1}, respectively. The outer boundary velocity was chosen to correspond to the blue edge of the Ca II λ3945 multiplet. The Ca II λ3945 multiplet absorption in the day −7/6/5 spectrum is the broadest observed in the SN 1992A spectra, and thus the outer boundary velocity is a lower limit on the highest ejecta velocity of SN 1992A. The electron scattering photosphere was located at 10,600 km s^{-1}. We have artificially turned the Ti II lines off in the calculation, since this gave a better fit to the UV region (see below).

The near-UV region (i.e., ∼2650–3650 Å) is largely formed by a complex blend of iron peak element lines. Consequently, interpretation depends on calculated synthetic spectra. The synthetic UV region is formed principally in the range 13,000–20,000 km s^{-1}, with some influence of the matter moving faster than 20,000 km s^{-1}. The absorption-like feature at ∼3050 Å has significant contributions from Cr II and Fe II; the absorption-like feature at ∼3250 Å has significant contributions from Cr II, Mn II, and Fe II. The ions Co II and Ni II make no significant contribution to the synthetic spectrum because

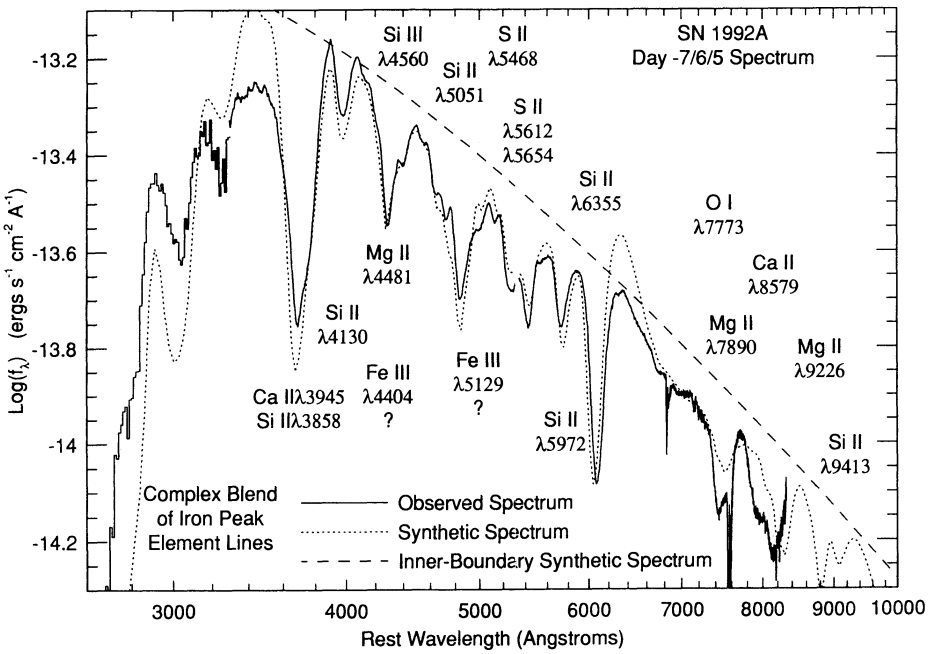

FIG. 7.—Observed and synthetic spectra for day −7/6/5 (1992 January 12–14 UT) of SN 1992A. The *IUE* and optical spectra that make up the observed day −7/6/5 spectrum are in their correct locations. Because the *IUE* spectrum is from day −5 and the adjacent ends of the *IUE* and optical spectra are somewhat uncertain, the apparent near-joining of the two spectra is probably somewhat coincidental. By extrapolation the day −6 UV spectrum could have been perhaps ~0.1 dex lower in the ~3200–3300 Å range than the day −5 *IUE* spectrum.

the newly synthesized Ni-Co is almost entirely confined below ~14,000 km s^{-1}; it is not obvious that newly synthesized Ni-Co would be helpful in forming the near-UV region. The ~3250 Å absorption-like feature in the synthetic spectrum would be largely smoothed away by the contribution of Ti II lines; It is because of this that we have artificially turned off the Ti II lines. Since titanium certainly exists in the supernova both from the explosive burning and from preexplosion abundance, the bad effect of Ti II lines on the synthetic spectrum fit is probably due to an incorrect temperature profile or to the limitation of the calculation to LTE conditions. Since Ti II has the lowest ionization energy of all iron peak element singly ionized species, except for Sc II, one can imagine a temperature or NLTE effect that affects mainly Ti II.

Because of the complexity of the line blend forming the UV region and because the fit is of only moderate quality, our interpretation is not very certain. Alternative ways of constructing this region are possible. For example, with a more steeply falling temperature profile or larger ϵ-value than the one we have used, the unmodified DD4 composition can be made to give a reasonable fit to the UV region, although perhaps not to the Ca II λ3945 absorption. A steeper temperature profile or large ϵ would compensate for the fact that the iron peak elements in the unmodified DD4 composition are effectively confined below ~14,000 km s^{-1}.

Although the sample of Type Ia optical spectra from ~7 days before maximum light is small, it seems that the optical day −7/6/5 spectrum is typical. For instance, the well-observed typical Type Ia SN 1989B had a very similar spectrum at a comparable epoch (Barbon et al. 1990; Phillips et al. 1992, Fig. 4*a*; Wells et al. 1993). The synthetic spectrum fit to the optical is good, and we are quite confident of the identifications we have made. Most of these identifications are well known (e.g., Branch et al. 1982; JLK). A few remarks on the optical spectrum formation should be made.

The outer boundary velocity of 31,000 km s^{-1} was not actually needed for our particular temperature profile (when extended beyond 31,000 km s^{-1}) and composition in order to keep the Ca II λ3945 multiplet absorption from being too broad. However, for other plausible choices of temperature profile, the cutoff would have been necessary. The Si II λ3858 multiplet is comparable in strength to the Si II λ6355 multiplet in LTE, but is often not commented on because it is expected to be less strong than the Ca II λ3945 multiplet. In our synthetic spectrum the Si II λ3858 multiplet is less strong, but not by a very large degree. The blue edge of the synthetic ~3700 Å absorption is, however, due to the Ca II λ3945 multiplet.

We have put question marks with the Fe III $\lambda\lambda$4404 and 5129 multiplet labels. These multiplets make an insignificant contribution to our synthetic spectrum, but with only slightly different atmospheric conditions they can be made to be significant. The small plateau region at about 5000 Å would in fact be better fitted if the Fe III λ5129 multiplet were stronger. That the Fe III multiplets can become very important in Type Ia's was established by the atypical Type Ia SN 1991T. In the premaximum optical spectra of this supernova, the Fe III $\lambda\lambda$4404 and 5129 multiplets caused the only strong optical P Cygni lines (Filippenko et al. 1992a; Ruiz-Lapuente 1992; Ruiz-Lapuente et al. 1992; JLK). It has been suggested that the strong Fe III lines in SN 1991T occurred because the outer layers (i.e., material above ~12,000 km s^{-1}) of this supernova were burned almost entirely to iron peak elements (Ruiz-Lapuente 1992; Ruiz-Lapuente et al. 1992). This suggestion cannot be entirely correct because there are oxygen and calcium in the outer layers (see § 8 and JLK); nevertheless, stronger burning in the outer layers of SN 1991T than in other Type Ia's is a

possibility. The Fe III λλ4404 and 5129 multiplets have also been found to be significant for the spectra of Type Ia SN 1990N (Ruiz-Lapuente 1992; JLK). For SN 1992A we find Fe III multiplets to be significant for the day +5/6 spectrum (see § 6.2). It is probable that the Fe III multiplets are significant at some epoch in most Type Ia's.

In the synthetic spectrum, the Mg II λ4481 multiplet forms the absorption centered at ~4290 Å. An observation of a Mg II λ9226 multiplet line, which is predicted by our synthetic spectrum, would have confirmed the Mg II λ4481 multiplet identification. Unfortunately, the observed spectrum does not extend far enough to the red to show a Mg II λ9226 absorption. We are aware of premaximum Type Ia spectra that extend far enough to the red to see this multiplet's absorption only for SN 1991T (Filippenko et al. 1992a; Ruiz-Lapuente 1992; Ruiz-Lapuente et al. 1992; Phillips et al. 1992; JLK), and these show no trace of a Mg II λ9226 multiplet line. Since SN 1991T had very atypical premaximum spectra, this null result says nothing about typical Type Ia's. Thus, the Mg II λ4481 identification, although very probable, is not completely confirmed; it is possible that the Fe III λ4404 multiplet is most responsible for the ~4290 Å P Cygni absorption.

The small absorption at ~4400 Å is fairly confidently identified with the Si III λ4560 multiplet. A similar absorption is seen in premaximum spectra of other typical Type Ia's and the atypical SN 1991T (e.g., Branch et al. 1982, 1983; Filippenko et al. 1992a, Fig. 4; Phillips et al. 1992, Fig. 4; JLK). Thus, a Si III λ4560 multiplet absorption is probably a common feature of most Type Ia's.

As expected (see § 5), the DD4 composition with newly synthesized silicon extending to ~25,000 km s^{-1} is able to reproduce the observed Si II λ6355 absorption's breadth. In fact, our synthetic fit to the Si II λ6355 absorption is a bit too broad. Perhaps model DD4 has too much silicon or too extended a silicon layer; however, a temperature error or NLTE effect may also account for the discrepancy. The large size of the emission feature of the synthetic Si II λ6355 multiplet P Cygni line is due to too large a value of ϵ for this multiplet. Our choice of $\epsilon = 0.1$ was, of course made to achieve an overall best fit.

The newly synthesized sulfur in model DD4 extends to ~23,000 km s^{-1}. The observed spectrum, however, neither demands nor rules out such fast newly synthesized sulfur. The observed S II lines arise from levels higher than 13 eV above the ground level, and thus are expected to form deep in the ejecta where the temperature is high. In the synthetic spectrum, the S II lines form below ~13,000 km s^{-1} where the temperature is higher than 8500 K.

The synthetic absorption near 7500 Å is much too weak. The blue side of the synthetic absorption is due to the O I λ7773 multiplet and the red side to the Mg II λ7890 multiplet. Unless the Mg II λ7890 multiplet is far out of LTE relative to the Mg II λ4481 multiplet, the synthetic O I λ7773 multiplet should be stronger. We were unable to find any plausible temperature profile that made the synthetic O I λ7773 multiplet sufficiently strong. It seems likely that a NLTE effect enhancing the O I λ7773 multiplet needs to be invoked. We discuss the near–7500 Å absorption further in §§ 6.2 and 8.

The synthetic Ca II λ8579 multiplet P Cygni line has a line velocity that is ~4000 km s^{-1} slower than the line velocity of the observed Ca II λ8579 multiplet line. Part of this discrepancy may arise from the fact that the region redward of ~7600 Å in the observed spectrum comes entirely from day −7, while most of the rest of the optical spectrum comes from day −6. Thus, a synthetic spectrum fit that weighted the day −6 observations more heavily than those of day −7 would be expected to have a Ca II λ8579 multiplet line velocity that was slow. However, an examination of the day −7 and day −6 spectra separately shows that the lines in common experienced slowing of line velocities of less than 1000 km s^{-1}. It seems likely that a NLTE effect is operating that strengthens the Ca II λ8579 multiplet (which arises from a metastable term) relative to the Ca II λ3945 multiplet.

6.2. *The Day +5/6 Spectrum*

Figure 8 shows the observed day +5/6 spectrum and the synthetic spectrum fit. For the synthetic spectrum fit the temperature profile shown in Figure 6 was used, ϵ was set to 0.1, and the inner and outer boundary velocities were 4250 and 22,000 km s^{-1}, respectively. The outer boundary velocity was chosen to keep the absorptions blueward of 3000 Å and the absorption due to the Ca II λ3945 and Si II λ3858 multiplets from being too broad. The electron scattering photosphere was located at 6500 km s^{-1}. We have again artificially turned the Ti II lines off in the calculation, since this gave a better fit to the 2650–3650 Å region (see below).

6.2.1. *The 1600–2900 Å Region*

The synthetic spectrum calculations show that the absorptions in the 1900–2900 Å region of Figure 8 are mainly formed in ejecta moving faster than ~16,000 km s^{-1}. Thus, the line formation in the synthetic spectrum calculation occurs in that region of the model where the iron peak elements have solar abundance and oxygen, silicon, magnesium, and sulfur dominate the composition. Because of strong line blending in the 1900–2900 Å region, it is impossible to determine the blue edges of individual lines. There is, however, no evidence for matter moving as fast as ~30,000 km s^{-1} from the 1900–2900 Å region; of course, ejecta at velocities greater than ~31,000 km s^{-1} may well exist (see § 6.1).

The synthetic fit we have obtained to the 1900–2900 Å region is not very good. The principal reason for this is the abrupt atmosphere cutoff we apply at 22,000 km s^{-1}. Experiments with gentle cutoffs (e.g., a steep exponential density decline above 20,000 km s^{-1}) give nicer fits. We have not presented these fits, since the prescriptions for them are even more arbitrary than the abrupt cutoff. If we move the abrupt cutoff farther out in the ejecta, the shape of the synthetic spectrum in the 1900–2900 Å region becomes much more like the observed spectrum, but the synthetic absorptions are all blueward of the observed absorptions. As one moves outward in supernova ejecta, the density falls and NLTE effects increase in strength. Probably these NLTE effects impose gentle cutoffs on the line opacities in the supernova.

The iron peak element multiplets we have identified in the 1900–2900 Å region are the strongest iron peak element multiplets (given a solar ratio of metals and the temperature law we have adopted). These multiplets all have lower terms which are low-lying metastable terms or ground terms. There is a great deal of line blending due to many weaker multiplets of many elements and to the fact that the lines of the dominant multiplets are often spread over tens of angstroms. In caution, it must be remarked that if the Fe II lines are turned off in the calculations, the other lines from singly ionized iron peak element ions and Si II combine to create a pattern of absorptions similar to what appears in Figure 8. Also, we found it possible to create a similar pattern with newly synthesized

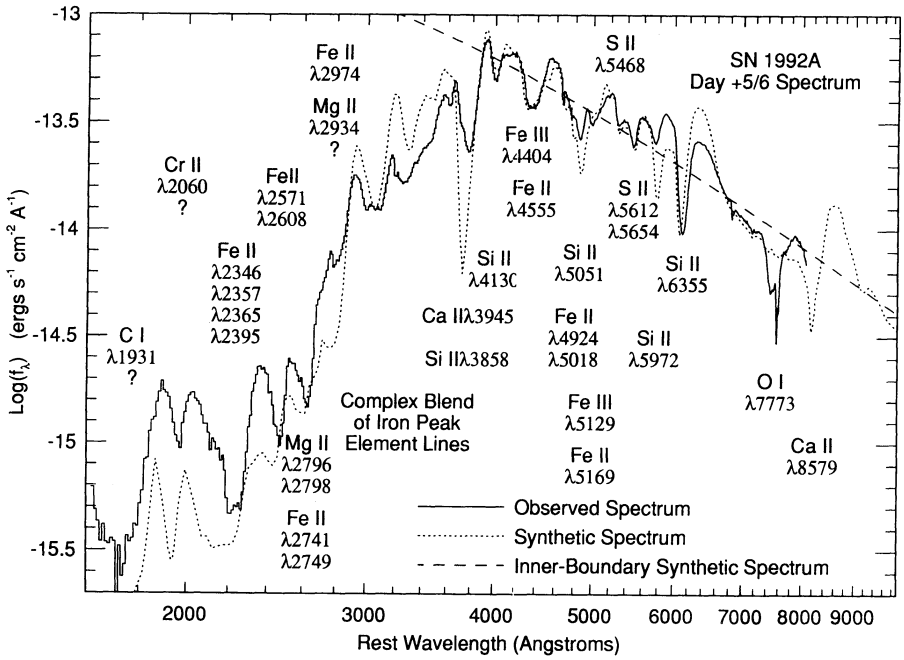

FIG. 8.—Observed and synthetic spectra for day +5/6 (1992 January 24–25 UT) of SN 1992A

Ni-Co dominating the iron peak element abundances. The iron peak element lines arising from a solar ratio of iron peak element abundances, however, give the best fit. Therefore, tentatively we conclude that a roughly solar ratio of iron peak elements exists above $\sim 16{,}000$ km s^{-1} in SN 1992A.

The Mg II λ2798 multiplet is very strong (it is a resonance multiplet) and for some plausible temperature profiles would largely form the absorption centered at 2630 Å even with only solar magnesium abundance. The contribution of the Mg II λ2934 multiplet to the small absorption at $\sim$2780 Å is less certain. Because they do not give rise to obvious line features, we have not indicated the Ni II multiplets in the 2180–2310 Å region in Figure 8. These multiplets have, however, a significant collective effect on the $\sim$2000–2250 Å region.

We have tentatively identified the absorption at $\sim$1975 Å as due to the Cr II λ2060 multiplet which arises from the ground term of Cr II. There are, however, contributions to this absorption from Co II, Fe II, and Zn II lines which for some sets of parameters may be as important as or more important than the Cr II λ2060 multiplet contribution.

The C I λ1931 multiplet makes a small contribution to the synthetic spectrum at $\sim$1800 Å. This multiplet has a low-lying metastable lower term and consists of only one line. We are not fitting the spectrum blueward of $\sim$1800 Å very well, and because of the spurious rise in flux toward 1600 Å we are not very certain of the flux level blueward of $\sim$1800 Å. Nevertheless, it seems clear that a strong C I λ1931 multiplet causing an absorption at $\sim$1800 Å (a wavelength blueshifted from 1931 Å by $\sim 20{,}000$ km s^{-1}) would not help our synthetic fit in this region. If the model DD4 ejecta had been carbon-rich outward from $\sim 15{,}000$ km s^{-1} (instead of outward from 23,000 km s^{-1}; see Fig. 4), the C I λ1931 multiplet would have been much stronger than it was in our calculations and would have caused more unneeded flux reduction at $\sim$1800 Å. Thus, there is at least weak evidence against carbon-rich ejecta below $\sim 23{,}000$ km s^{-1} in SN 1992A.

JLK very tentatively identified two C II lines in the earliest optical spectrum of SN 1990N, and Leibundgut et al. (1993), also very tentatively, identified a C I line in a postmaximum optical spectrum of the atypical Type Ia SN 1991bg. Besides this weak evidence for carbon lines, we know of no other empirical evidence for carbon in Type Ia's. The lack of solid evidence for carbon in Type Ia's is consistent with the delayed-detonation models (Khokhlov 1991a, b; Woosley 1991) and late-detonation models (Yamaoka et al. 1992), since in these models little carbon is left, at least below $\sim 20{,}000$ km s^{-1}, after the explosive burning.

6.2.2. *The 2650–3650 Å Region*

As in the day $-7/6/5$ spectrum, the day $+5/6$ observed spectrum in the near-UV region is largely formed by a complex blend of iron peak element lines. The synthetic spectrum in the 2650–3650 Å region in Figure 8 forms mainly in the 10,000–20,000 km s^{-1} range. In this range interpretation is complicated by abundance stratification of the iron peak elements: solar abundance in the fast layers and very enriched iron peak element abundance in the slow layers (see Fig. 4). We have found that enriched cobalt helps the fit to the region redward of $\sim$3200 Å; that cobalt can help to fit this region has been known for some time (Branch & Venkatakrishna 1986). However, because of the complicated line blending in the 2650–3650 Å region, we cannot say for sure in the case of SN 1992A that enriched cobalt is necessary. Even more than in the case of the fit to the day $-7/6/5$ spectrum (see § 6.1), we find that the Ti II lines worsen the fit, and this is the reason for leaving them out of the calculation again.

It is difficult to associate the features in the 2650–3650 Å region with any limited set of lines or multiplets. However, it seems probable that the small absorption at about 2780 Å is due mainly to the Fe II λ2974 multiplet with perhaps a contribution from the Mg II λ2934 multiplet. Although we do not fit the small absorption at 3610 Å with the displayed synthetic

spectrum, other synthetic spectrum calculations show that this absorption is probably due to one of, or some combination of, the Ca II λ3726 multiplet and the Co II λ3755 and Ni II λ3769 lines. The absorption is probably formed largely below $\sim$14,000 km s^{-1}, and thus in the region where the DD4 composition predicts enriched Ni-Co.

6.2.3. *The Optical Region*

The day +5/6 optical spectrum is very similar to those of most other Type Ia's observed at a similar epoch (e.g., Filippenko et al. 1992a, Fig. 5). Although the day +5/6 spectrum is clearly similar to the day −7/6/5 spectrum, some noticeable changes have occurred.

The absorption due to the Ca II λ3945 and Si II λ3858 multiplets has grown considerably narrower and has acquired a new shape. This new shape suggests that it is the Si II λ3858 multiplet which is primarily responsible for the blue side of the absorption. Our synthetic spectrum fit to the absorption is poor because the Ca II λ3945 multiplet is too strong and broad. When the Ca II lines are turned off in the synthetic spectrum calculation, the synthetic Si II λ3858 absorption does fit the blue side of the observed absorption nicely. A lower outer boundary velocity would have improved the fit to the observed absorption by making the synthetic Ca II λ3945 absorption narrower, but the 22,000 km s^{-1} cutoff was needed for fitting the observed absorptions blueward of 3000 Å. We could have accommodated both the need for a narrower synthetic Ca II λ3945 absorption and the region blueward of 3000 Å by using different outer boundary velocities in different wavelength regions; this, however, seemed too arbitrary a procedure to follow.

The synthetic Si II λ3858 multiplet may be too strong. Certainly the synthetic Si II $\lambda\lambda$5051, 5972, and 6355 multiplets are too strong; the Si II λ4130 multiplet may also be too strong, but this cannot be seen because of line blending.

The discrepancy between the observed and synthetic spectra in the $\sim$5700–6000 Å region, where the Si II λ5972 multiplet is the strongest contributor in the synthetic spectrum, is particularly noticeable. JLK suggested that a similar discrepancy in synthetic spectrum fits to spectra of SN 1990N and SN 1991T may be due to an early appearance of emission from the [Co III] λ5894 multiplet which gives rise to a true emission line identified in nebular epoch Type Ia spectra (Axelrod 1980a, b, 1988). This multiplet arises from the ground term of Co III. Moreover, in the Ni-Co-Fe core in the period from about 6 to 86 days after explosion, cobalt is the dominant element and Co III probably the dominant ion. Thus, although it is a forbidden multiplet, one might expect the [Co III] λ5894 multiplet to have an nonnegligible opacity. In the synthetic spectrum, the [Co III] λ5894 multiplet does in fact have a small effect but does not improve the fit. However, a NLTE effect increasing the emission from the [Co III] λ5894 multiplet (but not causing true nebular emission, since the densities are too high for this until $\sim$100 days after explosion) is probably the correct explanation for the flux deficiency of the synthetic spectrum in the $\sim$5700–6000 Å region. NLTE calculations confirm that [Co III] λ5894 emission does add extra flux in the $\sim$5700–6000 Å region as early as 10 days after maximum (Pinto 1992).

A dramatic change from the day −7/6/5 optical spectrum is the greatly increased importance of Fe II and Fe III multiplets and the insignificance of the Mg II λ4481 multiplet. This change is primarily due to the change in the temperature profile (see Fig. 6) and the recession of the line-forming region deeper into material rich in iron peak elements. The Fe III λ4404 multiplet helps form the blue side of the absorption centered at about 4350 Å, and the Fe III λ5129 multiplet contributes to the absorption at $\sim$5000 Å. The synthetic spectrum shows that the Fe III λ5876 multiplet contributes to the observed absorption at about 5750 Å; we do not fit this observed absorption very well, and so it is not clear that the Fe III λ5876 multiplet makes a contribution in the observed spectrum. In addition to the Fe II and Fe III multiplets, the synthetic spectrum calculations show that the Co II $\lambda\lambda$4152, 4302, 4479, 4607, and 4852 multiplets, and other Co II multiplets, make significant contributions in the $\sim$4000–5000 Å region.

In LTE the Mg II λ7890 multiplet will be less than a fifth as strong as the Mg II λ4481 for temperatures below 10^4 K. Since the $\sim$4350 Å absorption is well fitted without significant contribution from the Mg II λ4481 multiplet, we think that the synthetic spectrum is correct in predicting essentially no contribution to the near–7500 Å absorption from the Mg II λ7890 multiplet. In § 8 we rule out the possibility of Si II and S II multiplets contributing significantly to the near–7500 Å absorption. We conclude that the near–7500 Å absorption must be almost entirely due to the O I λ7773 multiplet even though our synthetic spectrum predicts an O I λ7773 multiplet that is a factor of $\sim$10–100 too weak.

As for day −7/6/5, we were unable to find a temperature profile that would make the synthetic O I λ7773 multiplet sufficiently strong, so we conclude that a NLTE effect is responsible for the strength of the near–7500 Å absorption. In A-type supergiant star atmospheres, which have temperatures similar to those we use for our Type Ia models, NLTE enhancements of the O I λ7773 multiplet's lower term occupation number by a factor of 10 are possible (e.g., Baschek, Scholz, & Sedlmayr 1977). An enhancement of the O I λ7773 multiplet's strength by a factor of 10 or more is plausible in Type Ia's where the NLTE effects might be larger than in A-type supergiant star atmospheres because Type Ia's have lower densities in their atmospheres. An expecially strong NLTE effect for the O I λ7773 multiplet's lower term results because this term is metastable and is the lowest quintet term of O I. There is no reason to expect other O I terms important for optical multiplets to be so strongly enhanced in Type Ia's, and the results of Baschek et al. (1977) for A-type supergiant star atmospheres tend to confirm this for the quintet terms. Thus, the lack of obvious line features due to other optical O I multiplets in Type Ia spectra is not a problem; these other multiplets even in LTE would be less strong than the O I λ7773 multiplet.

Even with a large departure coefficient for the O I λ7773 multiplet lower term, the DD4 composition (see Fig. 4) will produce an O I λ7773 multiplet absorption that fits only the blue side of the near–7500 Å absorption because high oxygen abundance is confined to velocities higher than $\sim$14,000 km s^{-1}. We discuss the near–7500 Å absorption and the O I λ7773 multiplet further in § 8.

6.3. *The Day +8/9 Spectrum*

Figure 9 shows the observed day +8 *IUE* and day +9 spectra which we have combined to form a day +8/9 spectrum and the synthetic spectrum fit; the two observed spectra are shown in their correct locations. For the synthetic spectrum fit, the temperature profile shown in Figure 6 was used, ϵ was set to 0.03, and the inner and outer boundary velocities were 3500 and 17,000 km s^{-1}, respectively. The outer boundary velocity

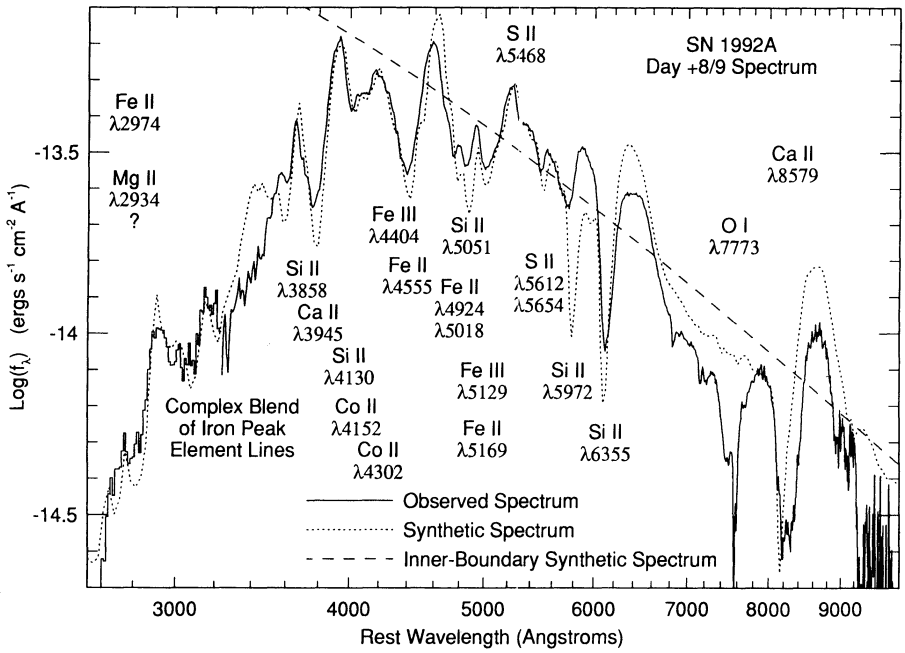

FIG. 9.—Observed and synthetic spectra for day +8/9 (1992 January 27–28 UT) of SN 1992A

was chosen to correspond to the blue edge of the observed Ca II λ8579 absorption. The electron scattering photosphere was located at 5200 km s^{-1}. For the synthetic spectrum we left the Ti II lines in the calculation, since in this case they seem to help the fit in the ~2900–3300 Å region.

A few interesting changes have occurred from the day +5/6 spectrum (see Fig. 5). The ~3500–5700 Å region has undergone a subtle alteration. Since we fitted this spectral region quite well on both days, we conclude that the composition stratification of model DD4 in the range ~7000–13,000 km s^{-1}, where most of the spectral region forms on both days, is reasonably good, except probably for a lack of oxygen (see §§ 6.2 and 8). Of course, the model W7 had a similar composition in the range ~7000–13,000 km s^{-1} (see, e.g., Branch et al. 1985, Fig. 2), and so would probably give good fits also.

As with the fit to the day +5/6 spectrum, the Si II λλ5051, 5972, and 6355 multiplets are too strong. The [Co III] λ5894 multiplet makes a significant contribution to the synthetic spectrum in the ~5700–6000 Å region that makes the fit worse; we expect, however, that NLTE emission from this multiplet accounts for the difference from the observed spectrum. The near–7500 Å absorption is again completely unfitted by the synthetic spectrum, and again we assume that the O I λ7773 multiplet strengthened by a NLTE effect accounts for this absorption. The synthetic Ca II λ8579 P Cygni line has too much emission with $\epsilon = 0.03$. The Ca II λ8579 multiplet is clearly more nearly a pure scattering line; $\epsilon = 0.01$ gives a much better fit to the observed Ca II λ8579 P Cygni line, but a somewhat poorer fit blueward of ~4000 Å.

The observed spectrum is not fitted at all redward of ~9200 Å. The observed spectrum, however, is poor in this region and is not to be trusted. Other Type Ia's observed at a comparable epoch do not provide us with a consistent picture of what the spectrum redward of ~9000 Å should look like. SN 1990N and SN 1991T spectra show a decline from the Ca II λ8579 emission to ~9500 Å that, allowing for noise, does not seem to show any clear line features (Filippenko et al. 1992a). However, infrared spectra from 12 to 15 days after maximum from SN 1989M and SN 1990M, respectively, show an absorption at ~9200 Å (Lynch et al. 1992). We have not yet been able to identify this absorption.

6.4. *The Day +45/47 Spectrum*

Figure 10 shows the observed day +45/47 spectrum and the synthetic spectrum fit. For the fit, we used the temperature profile shown in Figure 6, ϵ was set to 0.1 below 10,000 km s^{-1} and to 10^{-7} above 10,000 km s^{-1}, and the inner and outer boundary velocities were 3000 and 14,000 km s^{-1}, respectively. In achieving a synthetic spectrum fit in this case, we found using different ϵ-values for the inner and outer regions useful. The outer boundary velocity was chosen to prevent Mg II λ2798 multiplet emission in the synthetic spectrum from being too large; the outer boundary velocity one would get from Ca II λ3945 multiplet absorption blue edge is ~16,000 km s^{-1}. There was no electron scattering photosphere in the model: i.e., the electron scattering optical depth to the center of the ejecta was less than $\frac{2}{3}$. Logically, we should have set the inner boundary velocity to zero and relied purely on line emission to provide the flux. The current limitations of our computer code, however, required a finite inner boundary velocity; 3000 km s^{-1} seemed an adequate choice for synthetic spectrum fits. The Ti II lines have been included in the calculations. They slightly worsen the fit in the ~4000–4600 Å region and have a rather neutral effect in the UV region.

The synthetic spectrum fit we have obtained is not formally a best fit but only a reasonable fit, and the parameters are quite uncertain estimates of the physical conditions in SN 1992A. Increased uncertainties relative to those of our fits to earlier spectra result from the increasing importance of NLTE effects with time and the complexity of the optical line blending at the day +45/47 epoch. The NLTE effects increase with time because the density is falling (and thus collision rates, which help to impose LTE, fall) and because of the recession, after about the time of maximum light, of the electron scattering photosphere into the Ni-Co-Fe core where local γ-ray deposi-

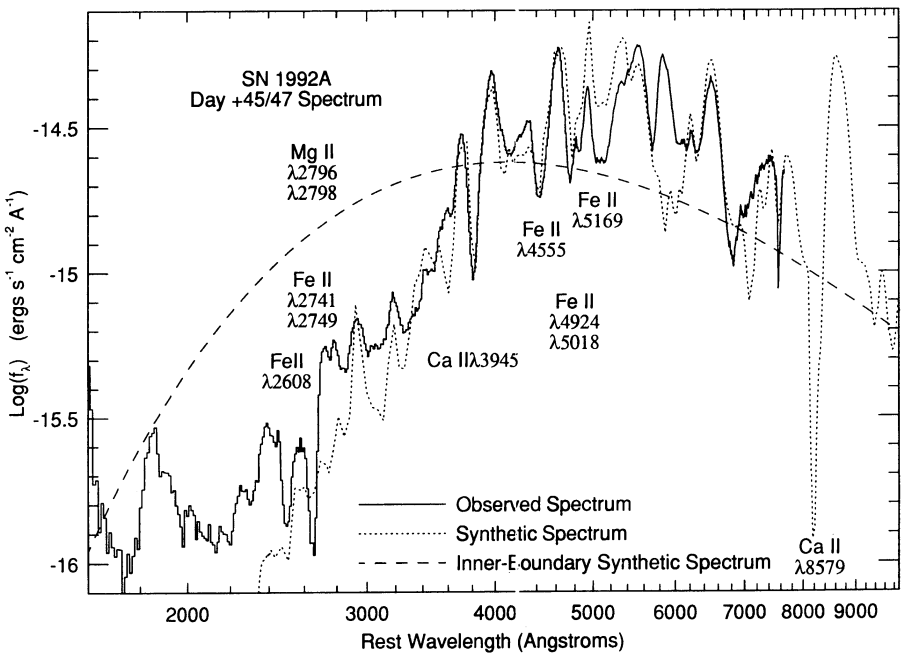

FIG. 10.—Observed and synthetic spectra for day +45/47 (1992 March 4–6 UT) of SN 1992A

tion is occurring. The local γ-ray deposition tends to cause NLTE line emission that is not subsequently thermalized in a low-density environment. The increased complexity of the optical line blending is a consequence of falling temperature that allows many optical lines of iron peak elements to become strong.

Because of the complexity of spectrum formation in both the UV and the optical at the day +45/57 epoch, we have indicated in Figure 10 only a very few of the strongest multiplets and lines that contribute to the observed spectrum. It would be difficult to sort out the relative importance of the contributions from other multiplets.

We obtain reasonable agreement with the observed spectrum redward of ~2500 Å. Blueward of ~2500 Å we obtain no fit at all, and thus we can say little about the features there. The synthetic spectrum blueward of ~2500 Å, which is mostly not displayed in Figure 10, falls increasingly below the observed spectrum in the blueward direction, shows only weak features, and does not resemble the observed spectrum. Probably the observed features blueward of ~2500 Å are the result of complex iron peak element line blending. Our failure to fit the region blueward of ~2500 Å probably occurred because we were unable to fine-tune the low flux level in this region while fitting the much larger flux in the near UV and optical.

The UV region probably forms above the Ni-Co-Fe core; inside the Ni-Co-Fe core the singly ionized iron peak element opacity is very large and probably enforces a continuum UV radiation field. The synthetic spectrum calculations suggest that multiplets of Ti II, Cr II, Mn II, Fe II, and Co II all make noticeable contributions in the UV; V II and Ni II have no noticeable effect on the synthetic UV region. Because we do not fit the UV region particularly well, we cannot say whether all these ions actually do contribute significantly to the observed spectrum.

We have only poor fits to the observed absorptions centered at ~2500 and ~2900 Å. As for the absorptions in the day +5/6 spectrum blueward of ~2900 Å, the principal reason for the poorness of the fits is probably the abrupt cutoff of the atmosphere (see § 6.2). The observed absorptions centered at ~2500 and ~2650 Å are probably mainly due to Fe II multiplets and the Mg II λ2798 multiplet. However, the synthetic spectrum analysis shows that Mn II and Co II multiplets probably also make significant contributions.

The small narrow bump at ~2780 Å in the observed spectrum varied during the accumulation of the spectrum and therefore cannot be due to the supernova. The rough correspondence of this bump and a bump in the synthetic spectrum is coincidental.

In the optical region Fe II and Co II cause most of the observed features. The optical iron peak element lines are probably formed mostly in the velocity range ~5000–12,000 km s^{-1}. The Ca II λ3945 multiplet absorption is clearly identified from the synthetic spectrum; the Ca II λ8579 multiplet absorption is certainly also present at this epoch, but was not covered in the observation. The Ca II λ3726 multiplet causes the synthetic absorption at ~3600 Å; this synthetic absorption is much too strong and must be largely suppressed in the observed spectrum by an NLTE effect. In the synthetic spectrum, the Si II λ6355 multiplet features have effectively disappeared because of the greatly increased strength of the Fe II lines, not because the Si λ6355 multiplet has weakened so much from earlier epochs. The synthetic Si II λ3858 multiplet still contributes to the synthetic absorption at ~3800 Å. Because no observed features can be attributed unambiguously to the Si II λλ3858 and 6355 multiplets, we do not know whether they in fact make any contribution to the observed spectrum.

Several features are not fitted by the synthetic spectrum. We do not obtain a fit to the ~5700–6100 Å region. We attribute this discrepancy, as at earlier epochs (see §§ 6.2 and 6.3), to NLTE emission from the [Co III] λ5894 multiplet. We estimate that the [Co III] λ5894 multiplet source function needs to be

~10–100 times its LTE strength in order to fit the observed emission feature; such a large departure from LTE does not seem improbable for a forbidden line in a semi-nebular epoch. The synthetic spectrum shows three absorptions due to Fe II lines in the ~6900–7700 Å region. None of these absorptions has an obvious counterpart in the observed spectrum. The small observed absorption at ~7000 Å may correspond to the much stronger synthetic absorption at ~7100 Å. The narrow observed feature at ~7575 Å is a telluric line, although a close examination shows that a slightly broader, shallower supernova absorption may be superposed on the telluric line; this possible supernova absorption may be the counterpart of the coincident synthetic absorption. The discrepancy in the ~6900–7700 Å region is probably just due to a slightly incorrect temperature or relatively small NLTE effects.

Because we do obtain partial agreement with the observed day +45/47 spectrum, and the discrepancies are not inexplicable given the limitations of the parameterized LTE procedure, we conclude that model DD4 is consistent with the day +45/47 spectrum.

Since the day +45/47 spectrum cuts off at ~7700 Å, it is interesting to compare our synthetic spectrum with an observed spectrum that extends farther to the red from another Type Ia at a similar epoch. In Figure 11 we show our synthetic spectrum compared with the day +50 spectrum of SN 1990N taken by Filippenko (Filippenko et al. 1992b, Fig. 9). The day +50 SN 1990N spectrum has been corrected for the NGC 4369 heliocentric velocity 983 km s^{-1} and for foreground Galactic extinction using $E(B-V) = 0.0125$ mag (Burstein & Heiles 1984) and the extinction law of Cardelli, Clayton, & Mathis (1989) with $R_V = 3.1$. This spectrum is very similar to the day +45/47 spectrum in the region of overlap; this is not surprising, since it is well known that Type Ia spectra from similar epochs, especially after maximum light, are very similar. The day +50 SN 1990N spectrum declines a little more slowly with wavelength redward of ~5200 Å and has much more distinct absorption features in the ~6900–7700 Å region than the day +45/47 SN 1992A spectrum. Note that the telluric line at ~7575 Å has been corrected for in the day +50 SN 1990N spectrum. The observed absorption features in the ~6900–7700 Å region in the day +50 SN 1990N spectrum clearly correspond to the synthetic spectrum absorptions in this region. This correspondence verifies the essential correctness of the synthetic spectrum predictions for the ~6900–7700 Å region. The observed Ca II λ8579 P Cygni line in the day +50 SN 1990N spectrum is reasonably well fitted by the synthetic spectrum.

Redward of ~9000 Å in the day +50 SN 1990N spectrum are three absorptions. Synthetic absorptions correspond to two of the observed absorptions; if the synthetic Ca II λ8579 emission were less strong, there would be a synthetic absorption corresponding to the third observed absorption. The three synthetic absorptions are due to complex blends of Fe II and Co II lines; these blends are certainly the cause of the observed absorptions.

The *J* band (effective wavelength 12,500 Å and effective width 3800 Å; e.g., Allen 1973) of Type Ia's in a period extending from at least 5 days to 110 days after maximum light shows a flux deficiency relative to a blackbody curve fitted to the optical and *H* and *K* bands (Leibundgut 1988; see also, e.g., Kirshner et al. 1973b; Branch et al. 1983). The infrared spectra of Type Ia's also show this flux deficiency (Frogel et al. 1987; Lynch et al. 1990, 1992). The cause of the deficiency well after maximum may be simply a lack of lines emitting flux in the *J* band (Pinto 1992); at earlier times, when Type Ia atmospheres are still thought to be photospheric, the deficiency is unexplained. When we extended our synthetic spectrum calculation into the infrared, we did not reproduce the deficiency; our infrared synthetic spectrum to ~14,000 Å consisted mostly of Fe II and Co II P Cygni lines superposed on the inner boundary comoving blackbody spectrum. Our use of an inner boundary continuum comoving blackbody spectrum does not allow us

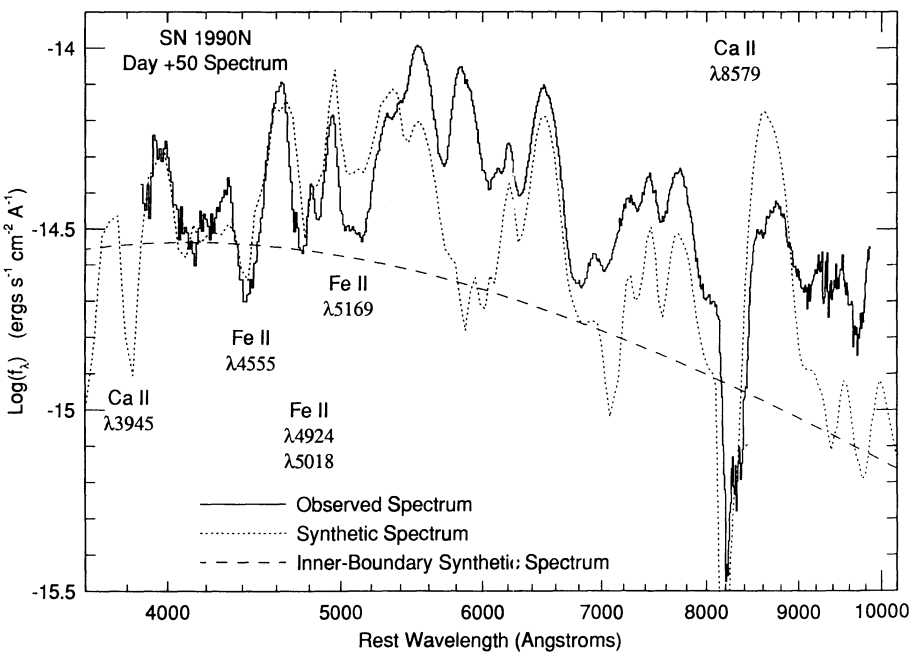

FIG. 11.—Observed spectrum for day +50 (1990 August 29 UT) of SN 1990N compared with the day +45/47 synthetic spectrum for SN 1992A

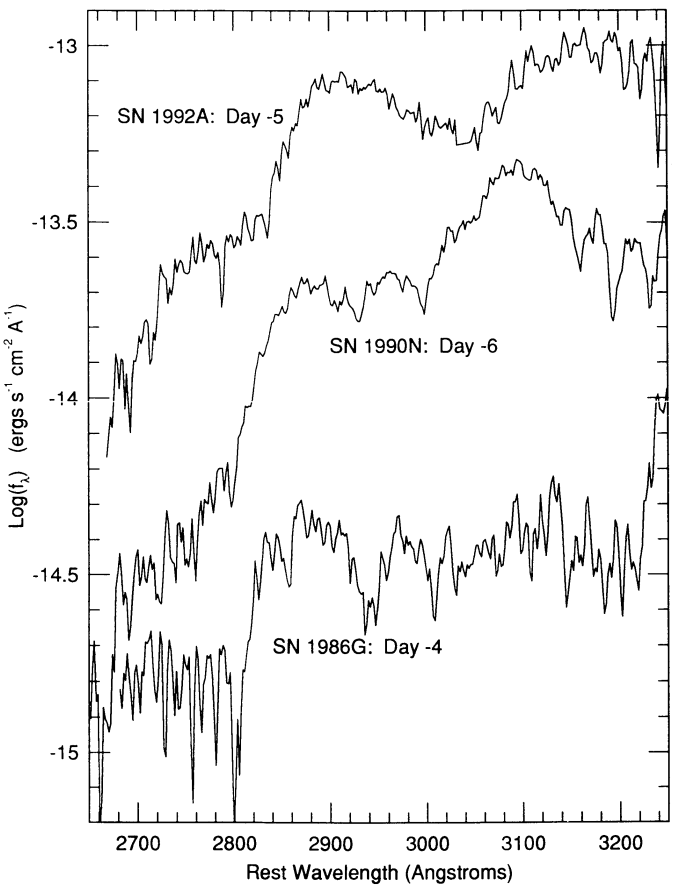

FIG. 12*a*

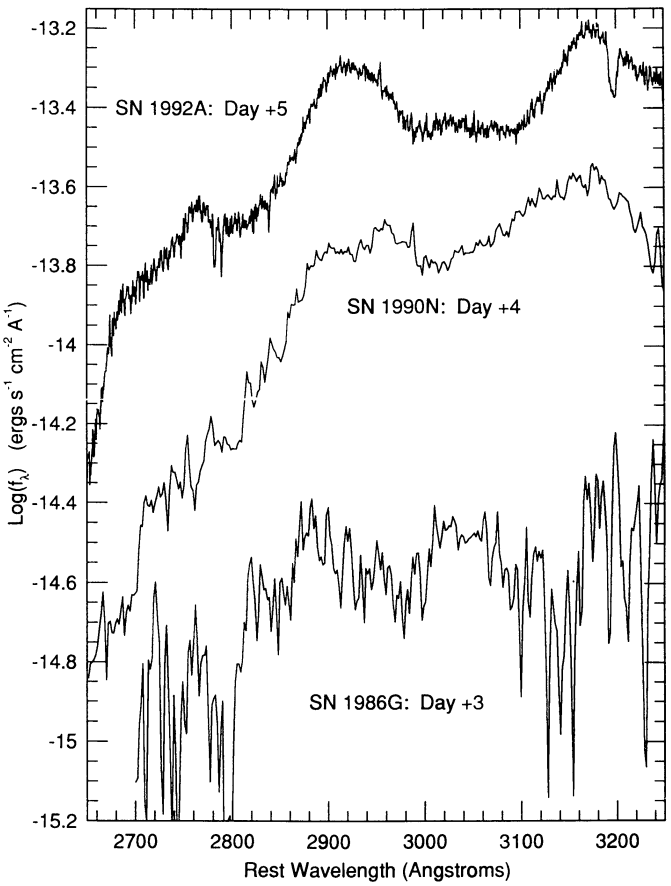

FIG. 12*b*

FIG. 12.—(*a*) Sample of premaximum Type Ia spectra from the wavelength region accessible by the *IUE*. The epoch of each spectrum relative to maximum light is indicated in the figure. The SN 1990N spectrum is in its correct position; the other spectra have been vertically displaced for clarity. (*b*) Same as (*a*), but for postmaximum Type Ia spectra.

the possibility of obtaining the flux deficiency from a lack of emitting lines.

7. THE 2650–3300 Å REGION OF TYPE Ia SPECTRA

The 2650–3300 Å region of Type Ia spectra has special importance because it is accessible with the *IUE* with good signal-to-noise ratio. Quality spectra from this region have been obtained for 11 Type Ia's including SN 1992A.[17] In most cases, however, only spectra from near-maximum light exist. The sample of *IUE* spectra is sufficiently large that a "typical" Type Ia 2650–3300 Å spectrum has been identified (Panagia & Gilmozzi 1991). The SN 1992A *IUE* and *HST* spectra conform to this typical spectrum, as do the *IUE* spectra of SN 1980N and SN 1981B (Panagia & Gilmozzi 1991, Fig. 1). Two Type Ia's, however, definitely do not conform: SN 1986G in NGC 5128 and SN 1990N in NGC 4639. SN 1986G was photometrically quite atypical, but its optical spectra were only a little atypical (Phillips et al. 1987). Aside from its *IUE* spectra, SN 1990N seems to have conformed in the main with our definition of a typical Type Ia (Leibundgut et al. 1991). The Si II and S II lines, most noticeably the Si II λ6355 line, of SN 1990N were weaker in the premaximum epoch than those of the typical SN 1989B (Phillips et al. 1992, Fig. 4*a*) and SN 1992A, but the sample of premaximum Type Ia spectra is too small to say whether this was atypical; in the postmaximum epoch, the SN 1990N Si II and S II lines seem of typical strength (Filippenko et al. 1992a, Fig. 5). Since we are uncertain about the importance of peculiarities of SN 1990N, we are uncertain at present whether it should be classified as typical or atypical.

Figures 12*a* and 12*b* compare *IUE* spectra from SN 1990N and SN 1986G with the *IUE* and *HST* spectra of SN 1992A: premaximum spectra are shown in Figure 12*a* and postmaximum spectra in Figure 12*b*. The SN 1990N *IUE* spectra have been corrected for heliocentric velocity and extinction just as we corrected the optical SN 1990N spectrum presented in § 6.4. The SN 1986G spectra were corrected for the NGC 5128 heliocentric velocity 541 km s^{-1} and for the estimated total extinction using $E(B-V) = 0.9$ mag (Phillips et al. 1987) and the extinction law of Cardelli et al. (1989) with $R_V = 3.1$. The

[17] There is an error in the *IUE* spectra of SN 1990N presented in the papers of Leibundgut et al. (1991) and JLK. All these spectra have a varying wavelength-scale error due to a mistake in smoothing; this error can be as large as ~50 Å. Furthermore, the *IUE* spectra labeled as coming from 1990 June 26 and July 3 actually came from 1990 June 28 and July 4, respectively, except in Fig. 3 of Leibundgut et al., where the epochs are correctly assigned. The synthetic spectrum fits of JLK to the SN 1990N spectra are improved by using the correct *IUE* spectra, except for the fit to the June 26 spectrum in JLK's Fig. 3*a*. The reasons for worsening of the June 26 fit may be significant, and we intend to investigate them in future work. We do not think, however, that the conclusions of the papers of Leibundgut et al. and JLK are affected by the errors made.

large extinction correction for SN 1986G decreases the overall slopes of the SN 1986G spectra somewhat and increases their overall flux scales by ~ 2 dex, but otherwise does not greatly affect them.

The spectra of the three supernovae in Figures 12*a* and 12*b* do not look alike at either epoch. The SN 1990N and SN 1992A spectra show time evolution clearly. Time evolution certainly also occurred in the case of SN 1986G, but even when examining the full set of six *IUE* spectra of SN 1986G spanning an interval of 23 days, time evolution is not very obvious because of the noisiness of the spectra. The single *IUE* spectrum with good signal-to-noise ratio available for the atypical Type Ia SN 1991T comes from about 1 day after maximum; this spectrum appears to be intermediate between the SN 1990N and the SN 1992A 2650–3300 Å spectra from comparable epochs. If the 2650–3300 Å region in the near-maximum light epoch is affected by newly synthesized Ni-Co (and JLK concluded that this was true for SN 1990N), then the differences in the 2650–3300 Å region among Type Ia's suggest that the outward extent of newly synthesized Ni-Co varies.

In the DD4 composition used for SN 1992A, newly synthesized Ni-Co dominates the iron peak elements only below $\sim 13{,}000$ km s^{-1}, where its effect on the 2650–3300 Å synthetic spectrum is obscured by the overlying colder material with solar iron peak element abundances. Since our synthetic spectrum fits to the 2650–3300 Å region are only of moderate quality, it is not clear from this spectral region that the outward extent of the newly synthesized Ni-Co in model DD4 is correct for SN 1992A. In our synthetic spectrum calculations for days +5/6, +8/9, and +45/47, much of the iron peak element line formation in the optical does occur below $\sim 13{,}000$ km s^{-1}. Since the optical synthetic spectra from these days (in which iron peak element lines are important) achieve reasonable agreement with the observations, there is some evidence that the modified DD4 iron peak element distribution with Ni-Co dominance only out to $\sim 13{,}000$ km s^{-1} is correct out to $\sim 13{,}000$ km s^{-1} and by extrapolation beyond $\sim 13{,}000$ km s^{-1}. In the case of SN 1990N, the synthetic spectrum analysis by JLK suggested that the shape of the SN 1990N *IUE* spectra was due to the dominance of newly synthesized Ni-Co over iron in the ejecta above $\sim 15{,}000$ km s^{-1}. Thus, very tentatively we conclude that newly synthesized Ni-Co extended farther in SN 1990N than in most Type Ia's. We have not yet done a synthetic spectrum analysis of SN 1986G.

8. THE IMPLICATIONS FOR TYPE Ia MODELS OF THE O I λ7773 LINE IN TYPE Ia SPECTRA

All Type Ia supernovae of which we are aware and which have wavelength coverage to at least ~ 8000 Å exhibit a moderately strong absorption centered near 7500 Å at least for some time before ~ 20 days after maximum. This absorption is usually attributed to the O I λ7773 multiplet with possible contributions from the Mg II λ7890, Si II λ7850, and S II λ7628 multiplets. The Si II λ7850 and S II λ7628 multiplets, however, would have to be at least 1.5 and 2 dex, respectively, stronger than LTE predicts relative to the observed strengths of the optical lines of Si II and S II to produce the near–7500 Å absorption alone, and thus they are probably not in fact significant at any epoch in a Type Ia evolution.

The Mg II λ7890 multiplet probably does make a significant contribution to the near–7500 Å absorption in at least some Type Ia's at some epochs. In our synthetic spectrum for day −7/6/5 of SN 1992A (see Fig. 7), the Mg II λ7890 multiplet makes about a 50% contribution to the synthetic near–7500 Å absorption, which is too weak by a factor of 2 or 3. For the Mg II λ7890 multiplet alone to have fitted the near–7500 Å absorption in this case, it would have to have been at least 20 times stronger than LTE predicts relative to the Mg II λ4481 multiplet, provided that the observed absorption near 4290 Å is in fact due entirely to the Mg II λ4481 multiplet. If the near–4290 Å absorption is in fact mainly due to the Fe III λ4404 multiplet, then it would be extremely unlikely that Mg II λ7890 multiplet is the main contributor to the near–7500 Å absorption. In the other epochs on SN 1992A that we analyzed, we found no significant Mg II λ7890 multiplet contribution (see §§ 6.2, 6.3, and 6.4).

Clear empirical evidence for a contribution from the Mg II λ7890 multiplet would be an observation of an absorption due to the Mg II λ9226 multiplet, since the upper term of the Mg II λ9226 multiplet is the lower term of the Mg II λ7890 multiplet. Unfortunately, the region where a Mg II λ9226 multiplet absorption would be expected (~ 8700–8900 Å) is seldom observed. Most of the observations of this region show no clear evidence for any Mg II λ9226 absorption (e.g., Filippenko et al. 1992a, Fig. 5), and thus show that the Mg II λ7890 multiplet is probably usually insignificant. The only case where a Mg II λ9226 absorption is clearly identified is in the day +1 spectrum of the atypical Type Ia SN 1991bg (Filippenko et al. 1992b); this absorption may also have had a contribution from the O I λ9264 multiplet. The shape of near–7500 Å absorption in the SN 1991bg spectrum shows evidence for the blending of two P Cygni lines (Filippenko et al. 1992b, Figs. 5, 6, and 7); the more redward of the contributing lines or multiplets is certainly the Mg II λ7890 multiplet. From the shape of the blended near–7500 Å absorption, it is unlikely that the Mg II λ7890 multiplet is the dominant contributor to this absorption. Moreover, the near–7500 Å absorption is stronger than the absorption attributed mainly to the Mg II λ9226 multiplet, and LTE would predict a weaker near–7500 Å absorption if the Mg II λ7890 multiplet were the overwhelmingly dominant contributor. Therefore, parameterized LTE analysis and direct empirical evidence (the observation or lack of observation of a Mg II λ9226 absorption) both suggest that the Mg II λ7890 multiplet cannot be the dominant contributor to the near–7500 Å absorption in Type Ia spectra. Having ruled out all other possible dominant contributors to the near–7500 Å absorption that we can think of, we conclude that this absorption must be mainly due to the O I λ7773 multiplet.

As we discussed in §§ 6.1 and 6.2, we are not very concerned by the fact that we achieve a poor fit (see Fig. 7) or no fit all (see Figs. 8 and 9) to the near-7500 Å absorption with the O I λ7773 multiplet. A NLTE effect can probably produce an increase in the strength of the O I λ7773 multiplet by a factor of ~ 10 or more (see § 6.2). Given this strong NLTE effect and a high oxygen abundance (i.e., $\gtrsim 0.1$ in mass fraction), an O I λ7773 multiplet absorption of the right order can probably be obtained. A NLTE calculation of the near–7500 Å absorption that used a mass fraction of 0.21 for oxygen produced an O I λ7773 multiplet absorption which was only somewhat too weak (Branch et al. 1991).

To be specific, we define an oxygen-rich layer to be a layer with oxygen mass fraction greater than or equal to 0.1. From the way in which burning occurs in the explosion model calculations, we believe it to be true that oxygen abundance will be falling very rapidly at the borders of oxygen-rich layers defined this way.

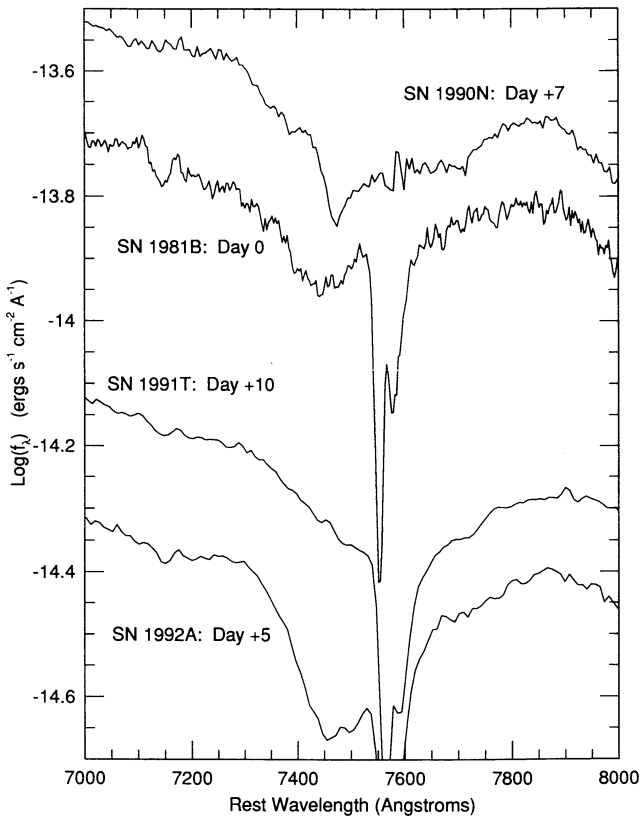

FIG. 13.—Type Ia spectra from the 7000–8000 Å region. The epoch of each spectrum relative to maximum light is indicated in the figure. The broad absorption is attributed principally to the O I λ7773 multiplet. The SN 1981B spectrum is in its correct position; the other spectra have been vertically displaced for clarity. The narrow absorptions at ~7575 Å seen in three spectra are telluric. The telluric absorption has been corrected for in the SN 1990N spectrum.

To find out where the oxygen-rich layer of Type Ia supernovae is located, we have examined the near–7500 Å absorptions of several Type Ia's at different epochs; Figure 13 displays some of these absorptions. All the spectra shown have been corrected for the parent galaxy redshift. The SN 1990N spectrum has been corrected for foreground Galactic extinction, just as we corrected the SN 1990N spectrum from a later epoch presented in § 6.4; the other supernovae had zero foreground extinction (Burstein & Heiles 1984). The deep narrow feature at ~7575 Å in three of the spectra is a telluric line; in the SN 1990N spectrum this telluric line has been corrected for. SN 1991T is atypical Type Ia as we have noted; the SN 1981B and SN 1992A are considered to be typical Type Ia's, and we are undecided about SN 1990N (see § 7). We take the blue edge of a near–7500 Å absorption as locating a lower bound on the outer extent of the oxygen-rich layer and the minimum of a near–7500 Å absorption as locating an upper bound on the inner extent of the oxygen-rich layer; this empirical way of determining bounds on the oxygen-rich layer should be consistent with our adopted definition of oxygen-rich layer (see above). (There are some cases where an absorption minimum can have a lower blueshift than the one corresponding to the slowest-moving matter in the line-forming layer [e.g., when one has a geometrically narrow line-forming layer immediately above a photosphere; e.g., Jeffery & Branch 1990, p. 192]. We do not think any of these cases apply to the near–7500 Å absorption of Type Ia's.) Because absorptions generally shift to the red with time, we tried to find the earliest and latest spectra showing the near–7500 Å absorption for determining the outer extent and inner extent bounds, respectively. We estimate the velocity determinations we make from the near–7500 Å absorption to be uncertain by at least 1000 km s^{-1}.

In Figure 13 the blue edges of all the absorptions, except perhaps for the SN 1981B absorption blue edge, are located at ~7300 Å, which requires oxygen moving at ~19,000 km s^{-1}. The SN 1981B blue edge is not very clearly defined and may be faster than ~19,000 km s^{-1}; a SN 1981B spectrum from a later epoch more clearly shows a blue edge indicating a velocity of ~19,000 km s^{-1} (Leibundgut et al. 1993, Fig. 7). Spectra showing a near–7500 Å absorption from earlier epochs than those shown in Figure 13, which are available only for SN 1991T (Filippenko et al. 1992a, Fig. 3) and SN 1992A (see Fig. 5), do not suggest any higher velocities.

The near–7500 Å absorption minima in spectra of SN 1981B and SN 1990N (e.g., Leibundgut et al. 1993, Fig. 7), and SN 1992A (see Fig. 5) from later epochs than those in Figure 13 suggest an upper bound on the inner extent of ~11,000 km s^{-1}. From these numbers, it follows that the oxygen-rich layer extends at least over the velocity range ~11,000–19,000 km s^{-1} in SN 1981B, SN 1990N, and SN 1992A.

For SN 1991T, the near–7500 Å absorption minima in Figure 13 and later spectra are blended with the telluric line; taking the blue edge of the telluric line as the location of the minima makes the upper bound of the inner extent ~9000 km s^{-1}. Thus, the velocity range of the oxygen-rich layer extends at least over ~9000–19,000 km s^{-1}. In the spectra of the atypical SN 1991bg, the O I λ7773 multiplet absorption is probably blended with the Mg II λ7890 multiplet absorption at least in the near-maximum epoch (see above and Filippenko et al. 1992b). Taking this blending into account, we infer from the spectra of Filippenko et al. (1992b) and Leibundgut et al. (1993) that the oxygen-rich layer in SN 1991bg extends over at least ~9000–16,000 km s^{-1}.

Other Type Ia supernovae (SN 1971L and SN 1972E [Kirshner et al. 1973a]; SN 1987D and SN 1987N [Filippenko et al. 1992a]) whose spectra we have examined are consistent with having oxygen-rich ejecta in the range ~11,000–19,000 km s^{-1}. In fact, SN 1972E (considered to be a typical Type Ia) showed evidence for oxygen-rich material extending over ~9000–22,000 km s^{-1}. The resolution of the SN 1972E spectra is rather low, and this probably adds another 1000 km s^{-1} to the uncertainty of the velocity determinations. From this limited survey of Type Ia's we conclude that typical Type Ia's have oxygen-rich ejecta at least in the range ~11,000–19,000 km s^{-1}.

The oxygen-rich layers that we have inferred impose strong demands on Type Ia models. Significant newly synthesized silicon must extend over at least the range ~10,000–19,000 km s^{-1} in typical Type Ia's and over at least ~10,000–25,000 km s^{-1} in some cases. (See § 5 for our choice of upper values for significant silicon abundance. The lower value of 10,000 km s^{-1} is based on Si II λ6355 line velocity studies of Barbon et al. 1990, Fig. 6, and Leibundgut et al. 1993, Fig. 9; these studies suggest that high silicon abundance may go deeper, but it is possible that line blending due to Fe II lines is invalidating the slowest line velocity determinations.) Moreover, in the case of SN 1990N, we think that newly synthesized Ni-Co must extend to at least ~15,000 km s^{-1} (JLK). Thus, newly synthesized

material, and oxygen, newly synthesized or preexisting, must coexist.

None of the current well-known models seems to satisfy these abundance conditions. Model W7 has an oxygen-rich layer extending from $\sim$13,000 km s^{-1} to the model cutoff at $\sim$22,000 km s^{-1}; given the uncertainties in our determination of oxygen-rich ejecta as slow as $\sim$11,000 km s^{-1} in typical Type Ia's, model W7 may be adequate to explain the near–7500 Å absorption in those cases. However, as noted in § 5 (see also § 6.1), model W7 has no newly synthesized silicon beyond $\sim$15,000 km s^{-1} and so must be ruled out. The model DD4, which we have used for the synthetic spectrum fits in § 6, is adequate to explain the SN 1992A spectra except that its oxygen-rich layer's lower bound is at $\sim$14,000 km s^{-1} (see Fig. 4). The other delayed-detonation models of Woosley (1991) had more extensive burning than model DD4; thus, their oxygen-rich layers begin at higher velocities than in model DD4, and they are less adequate than model DD4 to explain Type Ia spectra. We have not seen compositions for most of the delayed-detonation models of Khokhlov (1991a, b). However, none of his published model compositions, including the composition of his apparently favored model N21 (Höflich et al. 1992), seem to have oxygen-rich layers extending below $\sim$15,000 km s^{-1} (Khokhlov 1991b, Figs. 1 and 2). The sub–Chandrasekhar mass white dwarf detonation model for the Type Ia supernovae of Shigeyama et al. (1992) has its oxygen-rich layer's lower bound at $\sim$15,500 km s^{-1}. The late-detonation model W7DN of Yamaoka et al. (1992) has only an oxygen-rich layer extending outward from $\sim$29,000 km s^{-1} and a narrow oxygen-rich layer extending over $\sim$12,300–13,500 km s^{-1}. The other late-detonation models of Yamaoka et al. have no oxygen-rich layers at all, except for the oxygen-rich layer above $\sim$31,000 km s^{-1} in model W7DT.

The good properties of all the models we have just mentioned are that they have Ni-Co-Fe cores and, except for model W7 and some of Khokhlov's (1991a, b) delayed-detonation models, newly synthesized material extending to or beyond $\sim$20,000 km s^{-1}. It may be possible to preserve their good properties and have deeper oxygen-rich layers if a complex asymmetric burning front with relatively narrow random burning front fingers is invoked. Such a burning front could leave the unburned oxygen at deep layers (i.e., at $\sim$11,000 km s^{-1}). Alternatively, mixing could be invoked to spread oxygen to deep layers and newly synthesized elements into the outer ejecta. This mixing could be caused by some instability in the ejecta during the explosion, e.g., Rayleigh-Taylor instability in deflagration explosions (Nomoto et al. 1984). Extensive mixing during the explosion is expected to occur in Type Ia models in which the explosion results from the core collapse of a white dwarf (Colgate, Petschek, & Kriese 1980; Colgate 1991, 1992). Such models leave a neutron star remnant and eject less than 1 $M_\odot$. They are quite different from models that follow the standard Type Ia picture (where the explosion totally disrupts the white dwarf; see §§ 4 and 5), and we will not consider them further here.

To obtain physically realistic complex burning fronts or turbulent mixing, high-accuracy multidimensional calculations, which have not yet appeared, are needed. To investigate the effects of mixing on spectrum formation, calculations have been done using model W7 with an arbitrary homogenizing of the outer ejecta (e.g., ejecta above 8000 or 11,000 km s^{-1}) (Branch et al. 1985, 1991; Harkness 1991a, b; Ruiz-Lapuente 1992; Mazzali et al. 1993). These calculations reproduce reasonably well typical Type Ia spectra. However, such homogeneously mixed W7 compositions are poorer than unmixed W7 compositions for fitting the optical spectra of typical Type Ia's near maximum light (Harkness 1991a, b).

A problem with the complex burning front and mixing fixes for Type Ia explosion models is that Type Ia spectra have shown no evidence for aspherical inhomogeneities in the ejecta which one would expect in either case. (Recent two-dimensional calculations of turbulent burning in white dwarf explosion models suggest that large aspherical inhomogeneities will form if turbulent burning occurs [Livne 1993]. At present, such calculations have not achieved complete physical reliability, and so it is still possible that real turbulent burning yields approximately spherically symmetric ejecta.) Our synthetic spectrum calculations, for instance, do not suggest that any significant feature in the observed Type Ia spectra could not be reproduced by some choice of parameters with a spherically symmetric model. Although multidimensional synthetic spectrum calculations remain to be done, one would expect that gross aspherical inhomogeneities would lead to strange features that are not like those of ordinary P Cygni lines or line blends. For example, the satellite emission features that accompanied some of the P Cygni emissions in the spectra of the Type II supernova SN 1987A may have resulted from aspherical inhomogeneities (Cristiani et al. 1987; Hanuschik & Dachs 1987; Phillips & Heathcote 1989; Hanuschik & Thimm 1990; Hanuschik 1991). Of course, if the aspherical inhomogeneities resulting from complex burning or mixing are sufficiently small-scale, they may not give rise to strange features. As a guess, we would think that clumps near the photosphere of diameter $\sim$10% of the photosphere might cause strange features.

A third fix for the deflagration models, which avoids multidimensional calculations, may be to fine-tune the spherically symmetric model conditions to permit a deep, broad oxygen-rich layer and yet still have burning to $\sim$20,000 km s^{-1}. Model DD4 seems not so far from what is needed; perhaps some small adjustment of model DD4 will give an even more adequate model for the photospheric epoch spectra of typical Type Ia's. Given that model DD4 is also able to reproduce quite well the nebular epoch spectra of Type Ia's (Eastman & Pinto 1993; Pinto 1992), a little more work on delayed-detonation models of model DD4's kind may yield a very good Type Ia model.

9. THE SPHERICAL SYMMETRY OF TYPE Ia SUPERNOVAE

Type Ia's are usually assumed to be spherically symmetric for simplicity and tractability and also because no strong evidence of asymmetry has appeared. In § 8 we discussed the lack of spectral evidence for random aspherical asymmetries that might result from complex burning fronts or mixing. There might, however, be a smooth global asymmetry, e.g., a prolate or oblate asymmetry. Such a global asymmetry of the ejecta may not have any very obvious spectral signature even if the asymmetry is as large as $\sim$50% (Jeffery 1988, 1989, 1991b; Jeffery & Branch 1990). A detection of intrinsic Type Ia polarization, however, would be a clear signature of asymmetry; a spherically symmetric source, no matter how polarized the individual emergent beams, would always have an unpolarized net flux. The signature of intrinsic polarization would be time dependence or rapid wavelength dependence, especially if correlated with line features in the spectra. Interstellar polarization (ISP) is time-dependent and slowly varying with

wavelength. In distinguishing intrinsic polarization from ISP, spectropolarimetry and narrow-band polarimetry have the advantage over broad-band polarimetry in that rapid wavelength dependence is observable.

Because the optical continuous opacity of supernovae is dominated in some epochs by electron scattering which is polarizing, one expects that the optical radiation field emerging from supernovae will be polarized in those epochs. Besides providing a continuum polarization, the electron scattering gives rise to line polarization features (McCall 1984, 1985; Jeffery 1989, 1991a, b). Intrinsic continuum and line polarization was strikingly evident in the spectropolarimetry of the Type II supernova SN 1987A (Cropper et al. 1988; Bailey 1988; Jeffery 1991b, c). The intrinsic line polarization maxima of SN 1987A varied over the range $\sim$0.5%–4% (Jeffery 1991c). The intrinsic continuum polarization of SN 1987A varied in the range $\sim$0.1%–1.7% depending on wavelength and epoch (Jeffery 1991c). The analyses of SN 1987A polarization data (Méndez et al. 1988; Jeffery 1989. 1991a, b; Höflich 1991) suggest that SN 1987A had a global prolate or oblate asymmetry of $\sim$10%–20%.

For SN 1992A, spectropolarimetry has been taken by Spyromilio & Bailey (1993) for day +9 and day +47. The spectropolarimetry covers the range $\sim$4500–7250 Å and thus covers a substantial part of the optical region where polarized flux is most likely to be observed. No significant polarization was detected at any wavelength at either epoch. The noise in the data gave rise to an average polarization level of $\sim$ 0.3%. (Recall that polarization is a positive-definite quantity, and thus there will always be a nonzero average polarization if there is any random or systematic error even when there is no real signal.) Therefore, an upper limit on the observed continuum polarization and line polarization features is $\sim$0.3%. It would be possible to have intrinsic continuum polarization larger than $\sim$0.3% if the ISP toward SN 1992A partially canceled intrinsic polarization. However, based on the SN 1987A spectropolarimetry and polarimetry analyses, it seems unlikely that an intrinsic continuum polarization of $\gtrsim$0.3% could have existed without line polarization features of a comparable size also existing. Such features could be distorted, but not suppressed, by ISP. Therefore, we conclude that a $\sim$ 0.3% polarization is also an upper limit on intrinsic continuum polarization and line polarization features.

In light of the analyses of the SN 1987A polarimetry and a comparison of the SN 1987A and SN 1992A polarization data, we would estimate that any projected global asymmetry of SN 1992A would have to be less than $\sim$5%. If SN 1992A had an axis of symmetry with a small inclination angle relative to the line of sight, then the ejecta could actually have had a much larger asymmetry that 5%. The SN 1992A spectropolarimetry is, of course, consistent with complete spherical symmetry.

The only other spectropolarimetry of a Type Ia supernova was taken for SN 1983G (McCall et al. 1984; McCall 1985). The data were much noiser than the SN 1992A data; typically, the uncertainty in polarization at any wavelength was $\sim$1%–3% (in polarization, not in relative uncertainty). There was a mean polarization level of 2% $\pm$ 1% where the uncertainty is possible systematic uncertainty. It is possible that this mean level of polarization was due to ISP. The SN 1983G spectropolarimetry seems to show two polarization maxima associated with P Cygni absorptions; the observers, however, deemed these polarization maxima to be insignificant. Because of the noisiness of the data, the large possible systematic uncertainty, and the unknown amount of ISP, the spectropolarimetry of SN 1983G is inconclusive; there may or may not have been a large intrinsic polarization and a large asymmetry. There have been three Type Ia's for which broad-band polarimetry has been taken, but the results also seem rather inconclusive (see the reviews by Shapiro & Sutherland 1982 and Barrett 1988).

At the present, the best Type Ia polarimetry, the SN 1992A spectropolarimetry, supports the assumption that Type Ia supernovae are spherically symmetric. Since a detection of Type Ia asymmetry or a verification that Type Ia's (or most Type Ia's) are very spherically symmetric is a very important result for understanding the evolution and explosion mechanism of Type Ia's, further spectropolarimetric observations of Type Ia's are urged. Spectropolarimetric observations of supernovae of other types would likewise be important in studying those types.

10. CONCLUDING DISCUSSION

The larger the wavelength and time coverage of supernova photometry and spectra, the more constraints there are on supernova models. Thus, *HST* UV photometry and spectra are of great value because their UV coverage in wavelength is much larger than that of *IUE* photometry and spectra, and because they can be obtained at epochs when supernovae are much too faint for the *IUE*. Our *HST* observations are only a beginning in fulfilling the *HST*'s potential for supernova research. The *HST* photometry we have taken will help in determining the photometric evolution and bolometric luminosity of Type Ia's. The special importance of our *HST* spectra is a clear disclosure for the first time of the Type Ia spectral region blueward of $\sim$2650 Å. Our analysis of this spectral region has allowed us to identify P Cygni lines due to iron peak element multiplets and the Mg II λ2798 multiplet. Since these lines were predictable and were fairly easy to reproduce in our synthetic spectrum calculations, the greatest constraint provided by the *HST* data, spectroscopic and photometric, is probably the overall UV flux distribution. Since this UV flux distribution varies over $\sim$1.5 dex in the day +5 *HST* spectrum and over $\sim$1 dex in the day +45 *HST* spectrum, it could prove to be very difficult to fit in a self-consistent NLTE calculation without having the right model and the right physics.

In our high-resolution GHRS spectrum of SN 1992A, there is no detection of the interstellar medium of NGC 1380, and only a thin low-velocity interstellar medium is detected in the Galaxy. The presence of only a thin interstellar medium along the line of sight to SN 1992A is beneficial for the study of SN 1992A, since a thin interstellar medium implies that the complicating factor of extinction is probably negligible. However, for the study of the interstellar medium our GHRS spectrum is rather disappointing. Further GHRS observations of supernovae, however, may be much more illuminating about the interstellar medium. One need not rely on luck for obtaining supernovae heavily screened by interstellar media; such supernovae can be picked out by looking for evidence of strong interstellar lines in optical spectra.

The SN 1992A *HST* and *IUE* UV photometry we have taken in the F175W, F275W, and F342W bands gives light curves that are marginally consistent with uncertainty with the Type Ia template *U* light curve of Leibundgut (1988, 1993). Using data from SN 1992A and SN 1990N, we have constructed a Type Ia template *F275W light curve that is quite detailed from 14 days before maximum light to 22 days after

maximum light and that extends sketchily to 77 days after maximum light. The *F275W light curve is similar to, but probably not quite consistent with, the Type Ia template U light curve. In future work we intend to extend and improve the template *F275W light curve using the 1992 November 5 *HST* observations of SN 1992A and *IUE* data from other Type Ia's.

In this paper, we performed a parameterized LTE analysis of the SN 1992A spectra, including the *HST* and *IUE* spectra, that covers the period from day -7 to day $+47$. Despite the limitations of our analysis procedure, we believe that we can draw some valid conclusions about SN 1992A; since SN 1992A appears to be a typical Type Ia, our conclusions probably apply to all typical Type Ia's. We have determined that newly synthesized silicon must extend out in the ejecta to at least $\sim 19{,}000$ km s^{-1}. Other intermediate-mass elements that are synthesized at the same time as silicon must also extend out to at least $\sim 19{,}000$ km s^{-1}; these elements are probably mainly magnesium and sulfur, since an outer magnesium layer helps our synthetic spectrum fit to the day $-7/6/5$ spectrum and since sulfur and silicon are always produced together by burning. The synthetic spectrum calculations are consistent with a Ni-Co-Fe core boundary velocity of ~ 9000 km s^{-1}; that typical Type Ia spectra are consistent with a Ni-Co-Fe core boundary velocity of ~ 9000 km s^{-1} has, of course, been known for some time. We have also established that oxygen must be one of the dominant elements (i.e., have mass fraction $\gtrsim 0.1$) over at least the range $\sim 11{,}000$–$19{,}000$ km s^{-1} in typical Type Ia's. Nucleosynthesis that leaves a substantial oxygen abundance when producing a significant iron peak element abundance is difficult to imagine (Thielemann 1992). Thus, if large abundances of oxygen and newly synthesized iron peak elements coexist, then a complex burning front may have formed or some postburning mixing of the ejecta may have occurred. For SN 1992A we have not found it necessary to demand such coexistence, although we do not rule it out either. For SN 1990N, coexisting oxygen and newly synthesized iron peak elements may be required if JLK's conclusion of newly synthesized Ni-Co at $\gtrsim 15{,}000$ km s^{-1} in that Type Ia supernova is correct.

It is clear that a full study of the distribution of Type Ia's of newly synthesized iron peak elements above the Ni-Co-Fe core is needed. In such a study, Type Ia UV spectra (which are largely formed by iron peak elements) will be of great value. Since *HST* spectra of Type Ia's are likely to remain few in number and to have only very limited time coverage, an extensive comparative study of Type Ia UV spectra will be limited to the 2650–3300 Å region which is accessible with the *IUE* and the near UV regions that can be observed from the ground. The sample of available Type Ia *IUE* spectra is significant and remains to be fully analyzed. Nevertheless, the sample is still rather small and the time coverage, except for SN 1986G, SN 1990N, and SN 1992A, is not good. Since the *IUE* spectra of SN 1986G, SN 1990N, and SN 1992A are rather different from each other, it is clear that we do not know the full range of Type Ia UV behavior. Further *IUE* observations of Type Ia's with good time coverage are highly desirable.

The spectropolarimetry of SN 1992A by Spyromilio & Bailey (1993) is consistent with the common assumption that Type Ia's are spherically symmetric. Further spectropolarimetric observations of Type Ia's would help to verify or disprove this assumption. Either result would be of great value in understanding the evolution and explosion mechanism of Type Ia's.

Of all the models that we have considered, model DD4 (with the minor composition modification which we introduced) seems to be the closest to satisfying the spectroscopic constraints on a typical Type Ia model. This model was adequate for reproducing the spectra of SN 1992A as far as we can determine, except that the model DD4 oxygen-rich layer does not seem to reach deep enough in the ejecta. Because model DD4 is promising for both photospheric and nebular epoch spectra, further spectral analysis and explosion modeling with delayed-detonation models similar to DD4 seems worthwhile.

We thank Alex Filippenko for some SN 1990N spectra, Stan Woosley for his model DD4, Ken Nomoto and his collaborators for their late-detonation models, and Phil Pinto and Pilar Ruiz-Lapuente for helpful discussions. The referee's careful reading of this paper and suggestions are well appreciated. C. Winge thanks the Brazilian agency CNPq for a fellowship. The research for this paper has been supported by NSF grant AST 89-05529 and NASA grants NAG 5-841 and NAGW-1789.

REFERENCES

Allen, C. W. 1973, Astrophysical Quantities (London: Athlone)
Anders, E., & Grevesse, N. 1989, Geochim. Cosmochim. Acta, 53, 197
Axelrod, T. S. 1980a, In Type I Supernovae, ed. J. C. Wheeler (Austin: Univ. Texas), 80
———. 1980b, Ph.D. thesis Univ. California Santa Cruz
———. 1988, in Atmospheric Diagnostics of Stellar Evolution: Chemical Peculiarity, Mass Loss, and Explosions, ed. K. Nomoto (Berlin: Springer-Verlag), 375
Bailey, J. A. 1988, Proc. Astron. Soc. Australia, 7 (No. 4), 405
Barbon, R., Benetti, S., Cappellaro, E., Rosino, L., & Turatto, M. 1990, A&A, 237, 79
Barbon, R., Iijima, T., & Rosino, L. 1989, A&A, 220, 83
Barrett, P. 1988, MNRAS, 234, 937
Baschek, B., Scholz, M., & Sedlmayr, E. 1977, A&A, 55, 375
Benetti, S., & Barbon, R. 1991, in Proc. Tenth Santa Cruz Workshop in Astronomy and Astrophysics, Supernovae, ed. S. E. Woosley (New York: Springer-Verlag), 493
Benvenuti, P., Sanz Fernandez de Cordoba, L., Wamsteker, W., Macchetto, F., Palumbo, G. C., & Panagia, N. 1982, An Atlas of UV Spectra of Supernovae (Noordwijk: ESA)
Blades, J. C., Wheatley, J. M., Panagia, N., Grewing, M., Pettini, M., & Wamsteker, W. 1988a, ApJ, 332, L75
———. 1988b, ApJ, 334, 308
Branch, D. 1987, ApJ, 316, L81
Branch, D., Buta, R., Falk, S. W., McCall, M. L., Sutherland, P. G., Uomoto, A., Wheeler, J. C., & Wills, B. J. 1982, ApJ, 252, L61
Branch, D., Doggett, J. B., Nomoto, K., & Thielemann, F.-K. 1985, ApJ, 294, 619
Branch, D., Lacy, C. H., McCall, M. L. Sutherland, P. G., Uomoto, A., Wheeler, J. C., & Wills, B. J. 1983, ApJ, 270, 123
Branch, D., Pauldrach, A. W. A., Puls, J., Jeffery, D. J., & Kudritzki, R. P. 1991, in Proc. ESO/EIPC Workshop, SN 1987A and Other Supernovae, ed. I. J. Danziger & K. Kjär (Garching: ESO), 437
Branch, D., & Venkatakrishna, K. L. 1986, ApJ, 306, L21
Burstein, D., & Heiles, C. 1984, ApJS, 54, 33
Cadonau, R., Sandage, A., & Tammann, G. A. 1985, in Supernovae as Distance Indicators, ed. N. Bartel (Berlin: Springer-Verlag), 151
Cardelli, J. A., Clayton, G. C., & Mathis, J. S. 1989, ApJ, 345, 245
Colgate, S. A. 1991, in Proc. Tenth Santa Cruz Workshop in Astronomy and Astrophysics, Supernovae, ed. S. E. Woosley (New York: Springer-Verlag), 585
———. 1992, private communication
Colgate, S. A., Petschek, A. G., & Kriese, J. T. 1980, ApJ, 237, L81
Cristiani, S., Gouiffes, C., Hanuschik, R. W., & Magain, P. 1987, IAU Circ., No. 4350
Cropper, M., Bailey, J. A., McCowage, J., Cannon, R. D., Couch, W. J., Walsh, J. R., Straede, J. O., & Freeman F. 1988, MNRAS, 231, 695
de Boer, K., Grewing, M., Richtler, T., Wamsteker, W., Gry, C., & Panagia, N. 1987, A&A, 177, L37
Dupree, A. K., Kirshner, R. P., Nassiopoulos, G. E., Raymond, J. C., & Sonneborn, G. 1987, ApJ, 320, 597
Eastman, R. G., & Pinto, P. A. 1993, ApJ, 412, 731

Filippenko, A. V., et al. 1992a, ApJ, 384, L15
Filippenko, A. V., et al. 1992b, AJ, 104, 1543
Frogel, J. A., Gregory, B., Kawara, K., Laney, D., Phillips, M. M., Terndrup, D., Vrba, F., & Whitford, A. E. 1987, ApJ, 315, L129
Hamuy, M., Phillips, M. M. Maza, J., Wischnjewsky, M., Uomoto, A., Landolt, A. U., & Khatwani, R. 1991, AJ, 102, 208
Hanuschik, R. W. 1991, in Proc. Tenth Santa Cruz Workshop in Astronmy and Astrophysics, Supernovae, ed. S. E. Woosley (New York: Springer-Verlag), 26
Hanuschik, R. W., & Dachs, J. 1987, A&A, 182, L29
Hanuschik, R. W., & Thimm, G. J. 1990, A&A, 231, 77
Harkness, R. P. 1991a, in Proc. Tenth Santa Cruz Workshop in Astronomy and Astrophysics, Supernovae, ed. S. E. Woosley (New York: Springer-Verlag), 454
———. 1991b, in Proc. ESO/EIPC Workshop, SN 1987A and Other Supernovae, ed. I. J. Danziger & K. Kjär (Garching: ESO), 447
Höflich, P, 1991, in Proc. ESO/EIPC Workshop, SN 1987A and Other Supernovae, ed. I. J. Danziger & K. Kjär (Garching: ESO), 387
Höflich, P., Khokhlov, A. M., & Müller, E. 1991, A&A, 248, L7
Höflich, P., Müller, E., & Khokhlov, A. M. 1992, A&A, submitted
Horne, K. 1988, in New Directions in Spectrophotometry, ed. A. G. D. Philip, D. S. Hayes, & S. J. Adelman (Schenectady: Davis), 145
Huo, J., Hu, D., Zhou, C., Han, X., Hu, B., & Wu, Y. 1987, Nuc. Data Sheets, 51, 1
Hutsemékers, D., & Surdej, J. 1990, ApJ, 361, 367
Jeffery, D. J. 1988, Ph.D. thesis, McMaster Univ.
———. 1989, ApJS, 71, 951
———. 1991a, in Proc. ESO/EIPC Workshop, SN 1987A and Other Supernovae, ed. I. J. Danziger & K. Kjär (Garching: ESO), 257
———. 1991b, ApJ, 375, 264
———. 1991c, ApJS, 77, 405
———. 1993, ApJ, 415, 734
Jeffery, D. J., & Branch, D. 1990, in Jerusalem Winter School for Theoretical Physics, Vol. 6, Supernovae, ed. J. C. Wheeler, T. Piran, & S. Weinberg (Singapore: World Scientific), 149
Jeffery, D. J., Leibundgut, B., Kirshner, R. P., Benetti, S., Branch, D., & Sonneborn, G. 1992, ApJ, 397, 304 (JLK)
Karp, A. H., Lasher, G., Chan, K. L., & Salpeter, E. E. 1977, ApJ, 214, 161
Khokhlov, A. M. 1991a, A&A, 245, 114
———. 1991b A&A, 245, L25
Kirshner, R. P. 1989, in Particle Astrophysics: Forefront Experimental Issues, ed. E. B. Norman (Singapore: World Scientific), 219
Kirshner, R. P., Blades, J. C., Branch, D., Chevalier, R. A., Fransson, C., Panagia, N., Wagoner, R. V., & Wheeler, J. C. 1988, *HST* Proposal SINS: The Supernova Intensive Study, unpublished
Kirshner, R. P., Oke, J. B., Penston, M. V., & Searle, L. 1973a, ApJ, 185, 303
Kirshner, R. P., Willner, S. P., Becklin, E. E., Neugebauer, G., & Oke, J. B. 1973b, ApJ, 180, L97
Kurucz, R. L. 1991, in Stellar Atmospheres: Beyond Classical Models, ed. L. Crivellari, I. Hubeny, & D. G. Hummer (Dordrecht: Kluwer), 441
Leibundgut, B. 1988, Ph.D. thesis, Univ. Basel
———. 1993, in preparation
Leibundgut, B., Kirshner, R. P., Filippenko, A. V., Shields, J. C., Foltz, C. B., Phillips, M. M., & Sonneborn, G. 1991, ApJ, 371, L23
Leibundgut B., et al. 1993, AJ, 105, 301
Liller, W. 1992, IAU Circ., No. 5428
Livne, E. 1993, ApJ, 406, L17
Lynch, D. K., Erwin, P., Rudy, R. J., Rossano, G. S., & Puetter, R. C. 1992, AJ, 104, 1156
Lynch, D. K., Rudy, R. J., Rossano, G. S., Erwin, P., Puetter, R. C., & Branch, D. 1990, AJ, 100, 223
Mazzali, P. A., Lucy, L. B., Danziger, I. J., Gouiffes, C., Cappellaro, E., & Turatto, M. 1993, A&A, 269, 423
McCall, M. L. 1984, MNRAS, 210, 829
———. 1985, in Supernovae as Distance Indicators, ed. N. Bartel (Berlin: Springer-Verlag), 48
McCall, M. L., Reid, N., Bessell, M. S., & Wickramasinghe, D. T. 1984, MNRAS, 210, 839
Méndez, M., Clocchiatti, A., Benvenuto, O. G., Feinstein, C., & Marraco, H. G. 1988, ApJ, 334, 295
Mihalas, D. 1978, Stellar Atmospheres (San Francisco: Freeman)
Moore, C. E., & Merrill, P. W. 1968, in Partial Grotrian Diagrams of Astrophysical Interest (NSRDS-NBS 23; Washington, DC: GPO)
Nomoto, K., Thielemann, F.-K., & Yokoi, K. 1984, ApJ, 286, 644
Panagia, N., & Gilmozzi, R. 1991 in Proc. ESO/EIPC Workshop, SN 1987A and Other Supernovae, ed. I. J. Danziger & K. Kjär (Garching: ESO), 575
Paresce, F. 1990, *Hubble Space Telescope* Faint Object Camera Instrument Handbook, Version 2.0 (Baltimore: STScI)
Perlmutter, S., Marvin, H. J., Muller, R. A., Pennypacker, C. R., Sasseen, T. P., Smith, C. K., & Wang, L.-P. 1991 in Tenth Santa Cruz Workshop in Astronomy and Astrophysics, Supernovae, ed. S. E. Woosley (New York: Springer-Verlag), 727
Pettini, M., et al. 1982, MNRAS, 199, 409
Phillips, M. M., & Heathcote, S. R. 1989, PASP, 101, 137
Phillips, M. M., et al. 1987, PASP, 99, 592
Phillips, M. M., Wells, L. A., Suntzeff, N. B., Hamuy, M., Leibundgut, B., Kirshner, R. P., & Foltz, C. B. 1992, AJ, 103, 1632
Pinto, P. A. 1992, private communication
Ruiz-Lapuente, P. 1992, Ph.D. thesis, Univ. Barcelona
Ruiz-Lapuente, P., Cappellaro, E., Turatto, M., Gouiffes, C., Danziger, I. J., Della Valle, M., & Lucy, L. B. 1992, ApJ, 387, L33
Shapiro, P. R., & Sutherland, P. G. 1982, ApJ, 263, 902
Shigeyama, T., Nomoto, K., Yamaoka, H., & Thielemann, F.-K. 1992, ApJ, 386, L13
Sonneborn, G., & Kirshner, R. P. 1992, IAU Circ., No. 5430
Spyromilio, J., & Bailey, J. A. 1993, Proc. Astron. Soc. Australia, submitted
Spyromilio, J., Meikle, W. P. S., Allen, D. A., & Graham, J. R. 1992a, MNRAS, 258, 53P
Spyromilio, J., Stathakis, R. A., McNaught, R., Sadler, E. M., Freeman, F., & Cannon, R. D. 1992b, IAU Circ., No. 5428
Strömgren, B. 1948, ApJ, 108, 242
Suntzeff, N. B., Parker, J., Hunter, D., & Barnes, T. 1992, IAU Circ., No. 5432
Suntzeff, N. B., et al. 1993, in preparation
Suntzeff, N. B., & Roth, K. C. 1992, IAU Circ., No. 5429
Thielemann, F.-K. 1992, private communication
Thielemann, F.-K., Nomoto, K., & Yokoi, K. 1986, A&A, 158, 17
Tully, R. B. 1988, Nearby Galaxies Catalog (Cambridge: Cambridge Univ. Press)
Wagoner, R. V., Perez, C. A., & Vasu, M. 1991, ApJ, 377, 639
Wegner, G., & McMahan, R. K. 1987, AJ, 93, 287
Wells, L. A., et al. 1993, in preparation
Wheeler, J. C., & Harkness, R. P. 1990, Rep. Prog. Phys., 53, 1467
Wheeler, J. C., Harkness, R. P., Barkat, Z., & Swartz, D. 1986, PASP, 98, 1018
Wiese, W. L., Smith, M. W., & Glennon, B. M. 1966, in Atomic Transition Probabilities, Vol. 1, Hydrogen through Neon (NSRDS-NBS 4; Washington, DC: GPO)
Wiese, W. L., Smith, M. W., & Miles, B. M. 1969, in Atomic Transition Probabilities, Vol. 2, Sodium through Calcium (NSRDS-NBS 22; Washington, DC: GPO)
Woosley, S. E. 1991, in Gamma-Ray Line Astrophysics, ed. P. Durouchoux & N. Prantzos (Paris: AIP), 270
Yamaoka, H., Nomoto, K., Shigeyama, T., & Thielemann, F.-K. 1992, ApJ, 393, L55.